THE JOURNAL OF PHYSICAL CHEMISTRY B

Article

pubs.acs.org/JPCB

Experimental and Modeling Study of the Phase Behavior of (Methane + CO_2 + Water) Mixtures

Saif Z. S. Al Ghafri,[†] Esther Forte,[‡] Geoffrey C. Maitland,[†] José J. Rodriguez-Henríquez,[§] and J. P. Martin Trusler*,[†]

[†]Qatar Carbonates and Carbon Storage Research Centre, Department of Chemical Engineering, Imperial College London, South Kensington Campus, London SW7 2AZ, U.K.

[‡]Centre for Process Systems Engineering, Department of Chemical Engineering, Imperial College London, South Kensington Campus, London SW7 2AZ, U.K.

[§]Research Group TERMOCAL, Thermodynamics and Calibration, Department of Energy, University of Valladolid, Paseo del Cauce 59, E-47011 Valladolid, Spain

ABSTRACT: In this work we report phase equilibrium measurements on the system (methane + carbon dioxide + water) carried out with a high-pressure quasi-static-analytical apparatus. The measurements have been made under conditions of two-phase vapor−liquid equilibrium, three-phase vapor−liquid−liquid equilibrium (VLLE), and four-phase vapor−liquid−liquid−hydrate equilibrium. The compositions of three coexisting fluid phases have been obtained along eight isotherms at temperatures from (285.15 to 303.5) K and at pressures up to either the upper critical end point (UCEP) or up to the hydrate formation locus. Compositions of coexisting vapor and liquid phases have been obtained along three isotherms at temperatures from (323.15 to 423.15) K and pressures up to 20 MPa. The quadruple curve, along which hydrates coexist with the three fluid phases, was also measured along its entire length. The VLLE data obtained for this mixture have been compared with the predictions of the statistical associating fluid theory for potentials of variable range (SAFT-VR), implemented with the square-well potential and using parameters fitted to pure-component and binary-mixture data. Specifically, we used the SAFT-VR parameters reported by Míguez and co-workers [Míguez, J. M.; dos Ramos, M. C.; Piñeiro, M. M.; Blas, F. J. *J. Phys. Chem. B* **2011**, *115*, 9604]. The pressure along the quadruple curve was compared with the predictions of two different thermodynamic models. Furthermore, a detailed study of the ternary mixtures was carried out based on comparison with available ternary data of the type (CO_2 + *n*-alkane + water) and available data for the constituent binary subsystems. In this way, we analyzed the observed effects on the solubility when the *n*-alkane component was changed or a third component was added.

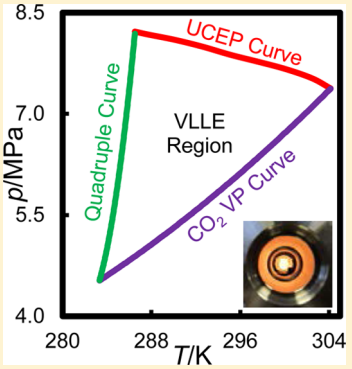

1. INTRODUCTION

An understanding of the phase behavior of mixtures containing hydrocarbons, CO_2, and H_2O is required to design effective and economic processes involving reservoir fluids and CO_2. Phase behavior data for these mixtures are key inputs to reservoir simulations that are used for evaluating reservoir-development plans, interpreting well-test data, and designing surface facilities and processing plants.[1] In addition, such data play a major role in the design of CO_2-storage and CO_2-enhanced oil recovery (EOR) processes.[2−12] In CO_2-EOR, displacement of oil by CO_2 is strongly affected by the phase behavior of the (oil + CO_2) system which, in turn, is dependent on reservoir temperature, pressure, and oil composition. In CO_2-storage processes, numerical simulations play a key role in predicting the flow of CO_2 from the injection wells into the storage formation and in determining the long-term evolution of the CO_2 plume after termination of injection. These simulations feed into larger geological/reservoir models which should provide an adequate representation of the storage process. In this way, proper selection and operation of storage sites can be accomplished with confidence. These geological/reservoir models require detailed thermophysical property data for CO_2 and its mixtures with the reservoir fluids it encounters, especially the phase behavior. To acquire all of the experimental data required over the range of reservoir temperatures, pressures, and fluid compositions involves an enormous amount of work. If existing predictive models can be validated with suitable accuracy, or new models developed, then this would greatly enhance the feasibility of CO_2-storage processes.[13]

In addition to carbon storage and CO_2-EOR, phase equilibrium data for mixtures containing CO_2 and hydrocarbons are significant in many industrial and scientific fields such as in hydrotreatment of aqueous waste streams,[14] production of coal liquids and petroleum processing,[15] separation processes,[16] and supercritical fluid extraction.[17,18] Large quantities of CH_4 are typically handled in reservoir production processes and CO_2 flooding projects; hence,

Received: September 24, 2014
Revised: November 17, 2014

   dx.doi.org/10.1021/jp509678g | *J. Phys. Chem. B* XXXX, XXX, XXX−XXX

Table 1. Literature Data of Ternary Mixtures of the Type (*n*-Alkane + CO_2 + H_2O)

ref	system	equilibria	T_{min}/K	T_{max}/K	p_{min}/MPa	p_{max}/MPa
32	CH_4 + CO_2 + H_2O	VLE	324.30	375.50	10.5	50.6
33	CH_4 + CO_2 + H_2O	VLE	344.15	344.15	10	100
34	CH_4 + CO_2 + H_2O	VLE	298.75	323.15	6.2	13.8
35	CH_4 + CO_2 + H_2O	VLE	243.1	288.4	0.11	6.05
35	C_2H_6 + CO_2 + H_2O	VLE	252.20	288.4	0.11	2.03
136	C_3H_8 + CO_2 + H_2O	VLE	247.50	289.00	0.1	2.1
28	C_3H_8 + CO_2 + H_2O	VLLE	311.10	353.18	1.67	6.71
136	C_4H_{10} + CO_2 + H_2O	VLE	252.90	288.30	0.1	2.1
29	C_7H_{16} + CO_2 + H_2O	VLLE	323.15	413.15	2	13
27	$C_{10}H_{22}$ + CO_2 + H_2O	VLLE	323.08	413.16	0.94	18.12
14	$C_{16}H_{34}$ + CO_2 + H_2O	VLLE	473.15	573.15	10.1	30.1

investigation of the impact of the presence of CH_4 on the mutual solubility of H_2O and CO_2 and on the CO_2 miscibility pressure are of both technical and economic significance.

Water is always found in oil-bearing geological formations. In the oil and gas industries, the H_2O content of the hydrocarbon phases often creates problems during transportation and processing, the most severe of which is the formation of gas hydrates which may block pipelines, equipment, and instruments. Pipeline conditions are typically in the temperature range of (253.15 to 323.15) K and the pressure range of (5 to 25) MPa, an envelope that includes states in which hydrates may form. CO_2 is also an important hydrate former because of its presence as a contaminant in natural gas.[19] Based on the combination and ratio of the hydrate formers, the structural and thermodynamic properties of the hydrates formed in mixed-gas systems can differ significantly from those with a single guest species. Because of this, a better understanding of the phase equilibria of mixed-hydrate systems is required in order to exploit the potential applications of hydrate formation in the presence of gas mixtures.

Methane in the form of hydrates is considered a potential source of energy, with conservative estimates suggesting that the energy stored in the form of hydrates exceeds all other hydrocarbon sources combined.[20] An extensive review of CH_4 hydrates as an energy source has been presented by Demirbas.[21,22] In addition, the enormous quantities of CH_4 stored as thermally unstable hydrates also causes an environmental concern associated with the high global warming potential of methane.[23] Hydrates have also been suggested as an economically advantageous alternative to liquefied natural gas (LNG) for transportation and storage of gas.[24] Furthermore, the use of CO_2 to displace CH_4 from natural hydrates is currently being explored as a means of simultaneous CH_4 production and CO_2 sequestration.[25] In all of these processes, knowledge of the phase equilibrium properties of the mixed gas hydrates systems is essential. A number of experimental devices, methods, and mathematical models implemented for the measurements and predictions of hydrate-rich phase equilibrium of various systems have been reviewed extensively by Sloan and Koh in their recent book.[26]

Because of the complexity of oil mixtures in which the components present are not all known, simpler systems that may represent certain characteristics of the real ones are usually studied. Unfortunately, experimental data for (hydrocarbon + CO_2 + H_2O) mixtures are scarce and typically limited to two-phase vapor−liquid equilibrium (VLE) measurements. Table 1 summarizes the published data for systems of the type (*n*-alkane + CO_2 + H_2O) together with the phases studied, and the pressure and temperature ranges. Studies of the three-phase vapor−liquid−liquid equilibrium (VLLE) regions are extremely limited. Brunner et al.[14] studied VLLE for the ternary mixture (*n*-hexadecane + CO_2 + H_2O) at temperatures of (473.15 and 573.15) K and pressures of (20.1 and 30.1) MPa using a static-analytical method. The phase compositions were all analyzed by gas chromatography. Forte et al.[27] measured the three-phase vapor−liquid−liquid equilibrium data of the ternary system (*n*-decane + CO_2 + H_2O) at temperatures from (323 to 413) K and pressures from (1 to 18) MPa using an analytical apparatus. The same authors[28] also studied the VLLE of the system (propane + CO_2 + H_2O) at temperatures from (311 to 353) K and pressures from (1.7 to 6.7) MPa, and Al Ghafri[29] has studied the mixture (*n*-heptane + CO_2 + H_2O) at temperatures from (323.15 to 413.15) K and pressures from (2 to 13) MPa using the same analytical apparatus. In the latter three cases, the experimental data obtained were compared with the predictions of the statistical associating fluid theory for potentials of variable range (SAFT-VR).[30,31]

Continuing from our previous studies of (*n*-alkane + CO_2 + H_2O) mixtures,[27−29] the present work is an experimental and modeling study of the ternary mixture (CH_4 + CO_2 + H_2O). The ternary mixture (CH_4 + CO_2 + H_2O) was the most widely studied system of the type (*n*-alkane + CO_2 + H_2O) both in the region of fluid-phase equilibria[32−35] and fluid−hydrate equilibria.[20,36−40] However, as shown in Table 1, previous fluid phase equilibrium measurements for this mixture were restricted to the vapor−liquid region only. The most recent study on this ternary mixture was that of Qin et al.[32] in which vapor−liquid equilibria were studied for different ratios of CO_2 to CH_4 at T = (324.3 and 375.7) K and p = (10 to 50) MPa. The effect of the gas-phase composition on the solubility of CO_2 and CH_4 in the aqueous phase was evaluated in terms of the apparent Henry's law constant $H_i = py_i/x_i$, where i denotes either CO_2 or CH_4, y_i denotes mole fraction in the gas phase, and x_i denotes mole fraction in the aqueous phase. It was found that the apparent Henry's law constant decreased with increasing ratio of CH_4 to CO_2 in the system, so that the CO_2 became more soluble by this measure upon the addition of CH_4. Similarly, it was found that, by the same measure, the solubility of CH_4 was enhanced by the presence of CO_2.

Jarne et al.[35] measured dew points of (CH_4 + CO_2 + H_2O) in the temperature range from (243.1 to 288.1) K at pressures from (0.11 to 6.05) MPa. The results obtained were analyzed in terms of a predictive excess-function equation of state. It was observed that the dew-point temperature at given pressure was highly dependent on the H_2O concentration but not strongly affected by ratio of CH_4 to CO_2. Dhima et al.[33] have measured

dx.doi.org/10.1021/jp509678g | J. Phys. Chem. B XXXX, XXX, XXX−XXX

the simultaneous and separate solubilities of CH_4 and CO_2 in H_2O at T = 344.25 K and pressures of (10 to 100) MPa and modeled their results using a combination of the Peng–Robinson equation of state (EoS) and Henry's law. In their study, it was observed that CO_2 solubility (as measured by the apparent Henry's law constant) increased in the case of the ternary mixture compared to that of the binary mixture. Similarly in a previous study,[32] it was also observed that the solubility of CO_2 increased as more CH_4 was present in the gas mixture.

Only in the work of Song and Kobayashi[34] were VLLE states measured, but only one phase was analyzed (the gas phase). In that work, the H_2O content in the CO_2-rich phase was analyzed, and it was concluded that the presence of the CH_4 lowered the H_2O content in the gas phase by 20% to 30% from that of pure CO_2.

Although a substantial amount of research has been carried out on mixed hydrates of CO_2 and CH_4, few studies report the compositions of the gas, hydrate, and all fluid phases. Table 2 summarizes the hydrate studies reported in the literature for the mixture of interest in this work. Belandria et al.[36] used a cylindrical equilibrium cell with sapphire windows for visual observation of hydrate formation. The apparatus was also fitted with a sampling device connected to a gas chromatograph for online phase composition analyses. However, only the gas phase was measured experimentally, while the compositions of the hydrate and aqueous phases were determined using a material balance approach in combination with the experimental data and the volumetric properties as evaluated from an EoS of the gas mixtures. In addition, the hydrate dissociation pressures were predicted (at the corresponding equilibrium temperature, CO_2 mole fraction in the gas feed, and H_2O mole fraction introduced to the system) using two thermodynamic models: CSMGem[26] (which is based on Gibbs energy minimization) and HWHYD[41] (which is based on equality of fugacity for each component throughout all phases present).

Table 2. Hydrate Equilibrium Data for the Ternary Mixture (CH_4 + CO_2 + H_2O)

ref	equilibria	T_{min}/K	T_{max}/K	p_{min}/MPa	p_{max}/MPa
38	H–V	273.06	280.46	2.0	3.5
36	H–L_w–V	273.6	284.2	1.51	7.19
37	H–L_w–V	275.14	285.34	1.92	7.47
42	H–L_w–V	273.56	283.26	1.5	5.0
39	H–L_w–V	280.3	280.3	3.04	5.46
20	H–L_w–V	274.02	280.1	1.66	4.03
40	H–L_w–V	258	274.1	0.5	3
43	H–L_w–L_{CO_2}–V	283.09	286.51	4.46	7.93
38,42	H–L_w–L_{CO_2}–V	283.32	285.56	4.53	6.72

Beltrán and Servio[37] also used a high-pressure pVT cell consisting of a very narrow glass tube for full visualization of the entire contents of the cell. They observed the hydrate, aqueous liquid, and vapor phases in equilibrium (H + L_w + V) at temperatures from (275.15 to 285.34) K and pressures from (1.92 to 7.47) MPa. However, they only measured the corresponding gas-phase compositions. Seo et al.[38,42] measured three-phase H + L_w + V equilibrium conditions at different gas feed compositions. They also measured the quadruple points at which four phases (H + L_w + L_{CO_2} + V) coexisted. In addition, two-phase equilibrium states of hydrate and vapor were measured and the concentration of CO_2 in the hydrate phase was also analyzed. Recently, Bi et al.[43] measured the four-phase (H + L_w + L_{CO_2} + V) equilibrium properties of the (CO_2 + CH_4) system using a view cell in the temperature range from (273.16 to 297.15) K at pressure up to 10 MPa. In their study, it was found that the four-phase region existed in the range of (4.46 to 8.4) MPa, (283.09 to 287.9) K, and (0 to 0.225) CH_4 mole fraction in the gas phase.

Thermodynamic models based on accurate experimental equilibrium data are needed to predict phase equilibria and hydrate thermodynamic properties for potential industrial applications. To be able to treat the nonsphericity of alkanes and the hydrogen-bonding interactions of H_2O, SAFT-VR[30,31] based on square-well potentials was used in the present study for VLLE calculations. The SAFT-VR intermolecular parameters were obtained from the work of Míguez et al.[44] In their work, they used SAFT-VR to estimate the global phase equilibrium diagram of the ternary mixture over a wide pressure and temperature range. Regarding hydrates, recently, Dufal et al.[45] integrated SAFT-VR into a traditional van der Waals and Platteeuw[46,47] (vdWP) framework for modeling clathrate hydrates; in this approach, SAFT-VR was used to describe the fluid phases while the vdWP method was used to model the hydrates themselves. In the present work, we make use of such a model to compare with experimental data. Additionally, the hydrate model (CSMHYD) developed by the Colorado School of Mines was also used.[48]

The binary systems (CO_2 + CH_4),[49−56] (CH_4 + H_2O),[32,57−77] and (CO_2 + H_2O)[33,60,64,66,78−110] have been covered extensively in the literature, both in terms of experimental phase equilibrium data and modeling approaches. A thermodynamic model developed by Duan et al.[111,112] for the solubility of CO_2 in water at temperatures of (273 to 533) K and pressures of (0 to 200) MPa was able to represent the CO_2 solubility data considered almost to within the experimental uncertainties. However, it is worth noting here that Hou et al.,[110] in their recent VLE measurements of (CO_2 + H_2O), found that the model gives increasing deviations from their data at temperatures above about 400 K. Spycher et al.[113] developed an alternative model for the mutual solubility of CO_2 and water at temperatures of (285 to 383) K and pressures up to 60 MPa. This model is able to represent the compositions of both the water-rich and the CO_2-rich phases to within the experimental uncertainties. In addition, Duan and Mao[114] developed a thermodynamic model for the binary mixture (CH_4 + H_2O) at temperatures of (273 to 523) K and pressures of (0 to 200) MPa which was also able to predict the CH_4 solubility to within the uncertainty of the available experimental data. We make use of these models in our analysis.

In the binary system (CO_2 + H_2O), the H_2O content in the gas phase decreases monotonically as pressure increases in the subcritical region. However, in the supercritical region, it decreases as pressure increases up to a pressure around (5 to 10) MPa and then increases again as pressure increases further. In all cases, the H_2O content in the gas phase increases as temperature increases. The CO_2 solubility in the H_2O-rich phase increases as pressure increases but decreases as temperature increases. For the binary system of (CH_4 + H_2O), the H_2O content in the gas phase decreases as pressure increases and increases as temperature increases while the CH_4 solubility in the H_2O-rich phase increases as pressure increases and decreases as temperature increases, similar to the behavior

dx.doi.org/10.1021/jp509678g | J. Phys. Chem. B XXXX, XXX, XXX–XXX

observed in the (CO_2 + H_2O) binary system. In this work, the effect of adding a third component on the behavior of these binaries is studied both experimentally and through modeling.

2. EXPERIMENTAL SECTION

2.1. Material. The CO_2 used in this work was CP grade supplied by BOC with a mole fraction purity higher than 99.995%. The CH_4 was supplied by BOC and was "low ethylene" grade with purity higher than 99.95%. The carrier gas used in the gas chromatography was CP grade helium from BOC with purity higher than 99.999%. The H_2O used was deionized to an electrical resistivity greater than 18 MΩ·cm at T = 298 K. The hydrogen was also supplied by BOC with purities higher than 99.995%. The tetrahydrofuran were supplied by Sigma-Aldrich with a purity of 99.9%. No purification was attempted.

2.2. Apparatus. In this work, we used the high-pressure quasi-static-analytical apparatus described in detail by Forte et al.[27] As shown schematically in Figure 1, the main components

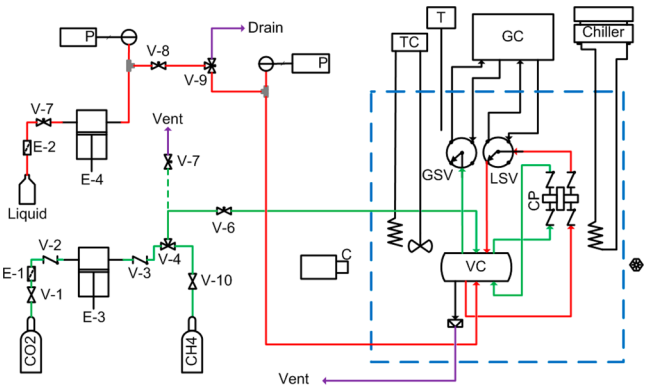

Figure 1. Schematic diagram of the analytical apparatus: E-3 and E-4, pumps; GC, gas chromatograph; VC, view cell; CP, circulating pump; TC, temperature controller; GSV, gas sampling valve; LSV, liquid sampling valve; P, pressure sensor; and T, temperature sensor. Red and green lines denote paths of liquid and gas phases, respectively.

were a high-pressure equilibrium cell, a magnetically coupled reciprocating circulation pump, electronically actuated sampling valves, a gas chromatograph (GC), and a temperature control system.

The equilibrium cell, made from type 17-4PH martensitic stainless steel, had a nominal internal volume of 35 cm^3 and was equipped with two diametrically opposite sapphire windows that enabled visual observation of the interior. The reciprocating pump was used for the circulation of both liquid and vapor, which was advantageous for promoting mass transfer between the phases. A chromatographic liquid sampling valve (LSV), with an internal 1 μL sample loop, was installed in the liquid recirculation loop and used to withdraw liquid samples for compositional analysis by GC. A chromatographic gas sample valve (GSV), with a 5 μL sample loop, was connected to the top of the equilibrium cell to enable sampling of the gas phase for analysis by GC. When two liquid phases were present, it was possible to tilt the cell such that the less-dense liquid was drawn into the recirculation loop; in that way the compositions of both liquids could be measured.

The transfer tubes connecting the sampling valves to the GC were heated by means of low-voltage mineral-insulated heater cables operating with K-type thermocouple temperature sensors and proportional-integral-derivative (PID) temperature controllers. During sampling, the components were vaporized on the heated transfer lines and transported to the GC column by the carrier gas. The GC was equipped with a thermal conductivity detector (TCD) connecting in series with a flame ionization detector (FID); the TCD was used for the detection of CO_2 and H_2O, while the FID was used for the detection of CH_4. A HayeSep Q column (80/100 mesh, 2 m long, 3.2 mm o.d, 2 mm i.d) was used to separate the three components. The operating conditions of the GC used in this work are listed in Table 3.

Table 3. Gas Chromatography Conditions for the Analysis of the Mixtures Used in This Work[a]

injector		column	TCD		FID	
$\dot{V}$/(cm^3·s^{-1})	T/K	T/K	T/K	I/mA	T/K	φ
40	423.15	343.15	523.15	90	523.15	1:10

[a]TCD = thermal conductivity detector; FID = flame ionization detector; $\dot{V}$ = He flow rate; I = current; φ = H_2/air flow ratio.

A manual syringe pump was used for the injection of liquid components into the equilibrium cell, while a refrigerated automatic syringe pump was used for the injection of liquefied CO_2. The CH_4 was admitted from the supply cylinder via a pressure regulator. The valves V-4, V-7, and V-9 shown in Figure 1 were used for the purposes of flushing, draining, and venting of the system. The temperature was controlled using a bath filled with silicon oil, a controller unit, and a stirrer. The bath was equipped with two double-glazed windows, at the front and back, which were aligned with the sapphire windows of the cell. A coil connected to an additional external refrigerated circulating bath was used to provide cooling when working at temperatures near or below ambient.

Back-illumination, using a light emitting diode source fitted with a diffuser, and a camera in front mounted on an optical rail facilitated the observation of the inside of the cell. The temperature was measured by means of a platinum resistance thermometer (PRT) located in the bath close to the equilibrium cell. The pressure was measured using a pressure transducer connected to the liquid inlet line through valve V-9. Prior to use, the system was thoroughly leak tested in the whole pressure range; it exhibited a high level of integrity. The system was also checked for leakage during the course of measurements.

2.3. Calibration. The pressure transducer was calibrated previously[27] against a pressure balance (Desgranges et Huot, model 26000) fitted with a piston-cylinder unit having a full-scale range of 50 MPa and standard relative uncertainty of 0.005%. The calibration was done in a range of pressures from (0.1 to 50) MPa, and the final standard uncertainty of the pressure measurements was estimated to be 5 kPa. No additional calibration was done for this work, and in order to account for any sensor drift over time, the pressure readings of the transducer were periodically compared at ambient pressure against a digital barometer located in the same laboratory and small additive corrections were made to account for the observed differences.

The PRT was also calibrated previously[27] on ITS-90 at the temperature of the triple point of H_2O and by comparison with a standard platinum resistance thermometer in a constant-temperature bath at temperatures up to 473 K. The standard

dx.doi.org/10.1021/jp509678g | J. Phys. Chem. B XXXX, XXX, XXX−XXX

uncertainty of the PRT was 0.01 K, but fluctuations of the bath temperature could be as much as ±0.05 K. Consequently the overall standard uncertainty of the cell temperature was estimated to be 0.05 K.

The TCD and FID were calibrated for each component individually by an absolute method using one of the sampling valves (LSV). In this method, we assume that the volume sampled by the LSV was always constant so that the amount of substance introduced into the GC was simply proportional to the density of the fluid at the sampling conditions. The calibration was carried out at the fixed column temperature at which measurements were performed and covered a range extending beyond the experimental measurements so that no extrapolation was performed on the calibration curves for any component.

The response of the TCD to varying amounts of CO_2 was determined by adjusting the conditions of pressure and temperature in the cell. The CO_2 density was obtained from the EoS developed by Span and Wagner[115] with an estimated relative uncertainty between 0.03% and 0.05% (which we interpret as an expanded uncertainty with coverage factor k = 2). For the sake of simplicity, we ascribe the value 0.025% to the standard relative uncertainty of the CO_2 density. Considering the reproducibility in the GC peak area, the standard relative uncertainty in the peak area for CO_2 was typically 1.0% while the standard relative uncertainty in the calculated amount of CO_2 at each given pressure and temperature was estimated to be 0.1%. As discussed below, the loop-volume uncertainty is excluded from this assessment.

The response of the FID to CH_4 was calibrated in the same way, and the density of CH_4 was obtained from the EoS developed by Setzmann and Wagner[116] with an estimated uncertainty ranging from 0.03% to 0.07%. Again, the standard relative uncertainty in the peak area was typically 1.0% while the standard relative uncertainty in the calculated amount of CH_4 at each given pressure and temperature was estimated to be 0.1%.

The response of the TCD to varying amounts of H_2O was calibrated by filling the equilibrium cell with gravimetrically prepared mixtures of H_2O and tetrahydrofuran. The calibration was carried out at a pressure just above ambient and at different temperatures for various mole fractions of H_2O. The mixture density was obtained from the work of Schedemann et al.[117] Considering the reproducibility in the response peak area, the standard relative uncertainty in the peak area response for H_2O was, on average, 2.0% while the standard relative uncertainty in the calculated amount of H_2O at each given pressure and temperature was estimated to be 0.2%.

As previously mentioned, TCD was used for both H_2O and CO_2. A linear relationship between the amount of H_2O present and the TCD response area was observed. However, in the case of CO_2, nonlinear behavior was observed at conditions where a large amount of CO_2 was present and a quadratic polynomial was therefore used for this component. The FID showed a very linear response for CH_4. From time to time during the course of the measurements, and also at the end of the work, the calibration was checked to ensure that no detector drift had occurred.

2.4. Experimental Procedure. The apparatus was initially cleaned with solvents, flushed with CO_2, and subjected to vacuum. H_2O, previously degassed under vacuum, was then loaded until it occupied approximately one-third of the cell volume, after which CO_2 was introduced slowly to the cell until the existence of three phases was observed. Finally, CH_4 was introduced slowly through valve V-4 until the desired initial pressure was reached at the given temperature.

The system was then left for at least 2 h to equilibrate while using the circulation pump to promote mixing. Once the system was equilibrated, the vapor phase was first sampled using the GSV. The H_2O-rich phase was sampled next by means of the LSV, and finally the cell was tilted to allow sampling of the middle CO_2-rich phase, again with the LSV. Further CH_4 was then injected so as to increase the pressure to the next state point, and the process was repeated for each isotherm. For each phase, at least six samples were taken and the results were examined to ensure reproducibility and to be sure that there was no evidence of cross-contamination or entrainment of one phase in the other or any sign of leakage. To locate precisely the UCEP at each temperature, the pressure was manipulated in very small steps by injecting or withdrawing H_2O while observing the phase state of the system. Close to the UCEP strong critical opalescence was observed. The phase compositions at the UCEP were measured by sampling at a pressure of approximately (0.01 to 0.02) MPa above the UCEP pressure.

For measurements of the four-phase H + L_w + L_{CO_2} + V locus, the system was initially brought to three-phase equilibrium. The temperature was then lowered until hydrates were observed to form. An equilibration period of at least 24 h was allowed before the temperature was slowly increased in steps of 0.01 K while monitoring both temperature and pressure. The point at which the slope of the $p(T)$ locus changed sharply was considered to be the point at which the hydrate crystals were fully dissociated and is reported as the hydrate dissociation condition. Similar procedures have been implemented in the literature.[36,118] It is worth noting here that, in hydrate measurements, there is usually a difference between the hydrate formation and dissociation conditions associated with metastability of the three-phase state during cooling. We note that, in the work of Bi et al.,[43] the temperatures and pressures of the four-phase states corresponding to the start and end of melting were identified. It was observed that the temperature change was small during melting but the pressure differences were considerable; our observations were similar.

During two-phase VLE measurements, the molar ratio between CO_2 and CH_4 in the gas phase was kept roughly fixed at about 0.5. This ratio was monitored by sampling the gas phase, and the composition was adjusted until the desired ratio was achieved.

2.5. Uncertainty Analysis. Using the guide to the expression of uncertainty in measurements (GUM),[119] the combined standard uncertainty of the mole fraction of each component in a given phase $u(x_i)$ is obtained from the following equation

$$u^2(x_i) = \sum_{j=1}^{n} \sum_{k=1}^{n} \frac{\partial x_i}{\partial z_j} \frac{\partial x_i}{\partial z_k} u^2(z_j, z_k) \tag{1}$$

Here, z_j and z_k are measured input variables, $(\partial u_i/\partial z_j)$ is the sensitivity coefficient of the input variable z_j, $u^2(z_j z_k)$ is the covariance $(j \neq k)$ or the variance $(j = k)$ for variables z_j and z_k. In this work, an absolute area method was used in which the peak area A_i in the chromatogram measured for component i in the mixture is related to the amount n_i of that substance in the sample. For the purposes of this uncertainty analysis, we

dx.doi.org/10.1021/jp509678g | J. Phys. Chem. B XXXX, XXX, XXX−XXX

assume that this relationship is linear and we define chromatographic response factors f_i such that

$$n_i = f_i A_i \tag{2}$$

The mole fractions x_i of each component are given by

$$x_i = n_i/(\sum_{k=1}^{N_c} n_k) \tag{3}$$

and hence may be obtained from the chromatographic peak areas and response factors as follows:

$$x_i = A_i f_i/(\sum_{k=1}^{N_c} A_k f_k) \tag{4}$$

Then considering eqs 1 and 4, the overall combined standard uncertainty of the mole fraction arising from temperature, pressure, response factor, and chromatographic peak area uncertainties is given by

$$u^2(x_i) = (\partial x_i/\partial T)^2 u^2(T) + (\partial x_i/\partial p)^2 u^2(p) + \sum_{j=1}^{N_c} \left(\frac{\partial x_i}{\partial n_j}\frac{\partial n_j}{\partial f_j}\right)^2 u^2(f_j) + \sum_{j=1}^{N_c} \left(\frac{\partial x_i}{\partial n_j}\frac{\partial n_j}{\partial A_j}\right)^2 u^2(A_j) \tag{5}$$

The partial derivatives, sensitivity coefficients, $(\partial x_i/\partial n_j)$ are given by

$$\left.\begin{aligned}(\partial x_i/\partial n_j) &= -x_i x_j/n_j \quad (j \neq i)\\ &= (1 - x_i)x_i/n_i \quad (j = i)\end{aligned}\right\} \tag{6}$$

and the partial derivatives (or sensitivity coefficients) $(\partial n_i/\partial f_j)$ and $(\partial n_i/\partial A_j)$ are given by

$$\left.\begin{aligned}(\partial n_j/\partial f_j) &= A_j\\ (\partial n_j/\partial A_j) &= f_j\end{aligned}\right\} \tag{7}$$

It follows that the overall standard uncertainty of x_i is given by

$$u^2(x_i) = (\partial x_i/\partial T)^2 u^2(T) + (\partial x_i/\partial p)^2 u^2(p) + \sum_{j\neq i} (x_i x_j)^2 [u_r{}^2(f_j) + u_r{}^2(A_j)] + [x_i(1 - x_i)]^2 [u_r{}^2(f_i) + u_r{}^2(A_i)] \tag{8}$$

where $u_r(X)$ denotes the standard relative uncertainty of variable X. The standard relative uncertainties in the response factors are given by

$$u_r{}^2(f_j) = [u_r{}^2(n_j) + u_r{}^2(A_j)]_{cal} \tag{9}$$

where subscript "cal" denotes the calibration measurement for component j. We note that, in the case of a binary mixture, eq 8 reduces to the following simpler form

$$u^2(x_1) = (\partial x_1/\partial T)^2 u^2(T) + (\partial x_1/\partial p)^2 u^2(p) + [x_1(1 - x_1)]^2 \sum_{j=1}^{2} [u_r{}^2(f_j) + u_r{}^2(A_j)] \tag{10}$$

In this analysis, the uncertainty of the sample-loop volume is not considered as it is assumed to be constant and therefore cancels in the analysis.

From eq 8, the overall combined uncertainty in the measured mole fraction of a component is affected by the uncertainties of pressure, temperature, response factor, and peak area. From eq 9, the uncertainty of the response factor of a component in the mixture is determined by the uncertainties during calibration of both the peak area and the calculated amount of substance for that pure component, the latter being affected by the uncertainties of pressure, temperature, and the equation of state from which the density is calculated. The typical standard uncertainties of all of the input variables have been given previousl, and these lead to overall combined standard uncertainties of mole fraction that vary over a wide range from 1×10^{-6} to 3×10^{-3} depending upon the component, temperature, pressure, and phase in question. It was observed that larger uncertainty occurs at lower temperatures and higher pressures.

2.6. Validation. The apparatus was validated in previous work by measuring the vapor−liquid equilibria of $(CO_2 + C_{10}H_{22})$[27] and $(CO_2 + C_7H_{16})$[29] and comparing the results with the available literature data; good agreement was found. In the present work, further validation measurements were undertaken on the $(CO_2 + H_2O)$ system at T = 323.15 K where measurements were made of the solubility of CO_2 in the water-rich phase at pressures up to 19 MPa. The results are given in Table 4 and are compared in Figure 2 with the available literature data.[79,80,82,87,93,99,110,120] Here, we observe good agreement over the entire pressure range.

Table 4. Experimental Solubility Data in the Water-Rich Phase for $(CO_2 + H_2O)$ at Temperature of 323.15 K

p/MPa	x_1	$u(x_1)$	x_2	$u(x_2)$
2.066	0.00642	0.00015	0.99358	0.00014
3.332	0.01003	0.00024	0.98997	0.00022
4.415	0.01269	0.00028	0.98731	0.00028
5.585	0.01561	0.00035	0.98439	0.00034
6.953	0.01758	0.00039	0.98242	0.00039
9.062	0.02004	0.00044	0.97996	0.00043
13.521	0.02173	0.00048	0.97827	0.00048
18.683	0.02280	0.00050	0.97720	0.00050

3. EXPERIMENTAL RESULTS

The binary system $(CH_4 + CO_2)$[121] exhibits type I phase behavior while the binary systems $(CO_2 + H_2O)$[108] and $(CH_4 + H_2O)$[122] exhibit type III phase behavior according to the classification of Scott and van Konynenburg.[123,124] As a consequence, the ternary mixture exhibits class IV behavior according to the global ternary diagram classification proposed by Bluma and Deiters.[125] Mixtures of this type possess an LLE immiscibility region, and hence, a VLLE region is also expected. The principal region of the present investigation is illustrated on a pressure−temperature diagram in Figure 3. The region within which three fluid phases coexist is bounded at low pressures by the three-phase $L_w + L_{CO_2} + V$ curve of the $(CO_2 + H_2O)$ binary system (which is almost coincident with the vapor pressure curve of pure CO_2), and at high pressures by either the UCEP locus $L_w + L_{CO_2} = V$ or the four-phase line along which hydrate coexists with the three fluid phases. Figure 3 also shows

dx.doi.org/10.1021/jp509678g | J. Phys. Chem. B XXXX, XXX, XXX−XXX

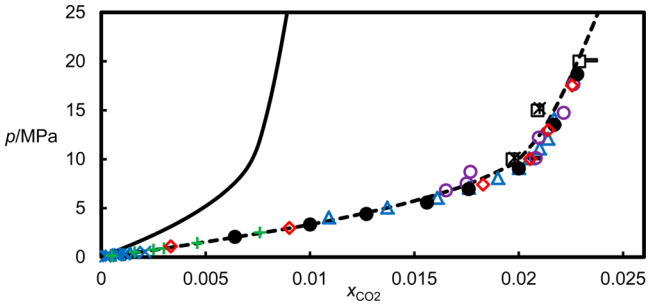

Figure 2. Isothermal pressure−composition (p, x) phase diagram at T = 323.15 K for the binary system (CO_2 + H_2O). The filled symbols correspond to the data gathered in this work at different pressures in the water-rich phase. The open symbols correspond to the binary published data for the following: ×, ref 99; □, ref 80; Δ, ref 79; −, ref 87; *, ref 120; ○, ref 82; +, ref 93; ◊, ref 110. The dotted and solid lines correspond to the solubility in the binary system (CO_2 + H_2O) obtained at the same temperature and different pressures from Duan et al.[112] and SAFT-VR[44] models, respectively.

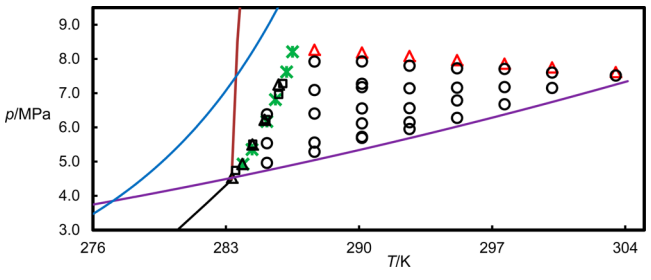

Figure 3. VLLE region and its boundaries: *, quadruple data gathered in this work; □, ref 43; Δ, refs 38 and 42; ○, VLLE data gathered in this work; Δ, UCEP data gathered in this work. Solid lines denote phase boundaries: CO_2 saturated vapor pressure (purple);[115] three-phase region L_w−H−V for the pure methane (blue);[128] three-phase region L_w−H−V for the pure CO_2 (black);[126] and three-phase region L_w−H−L_{CO_2} for the pure CO_2 (brown).[127]

the vapor-pressure curve of pure CO_2,[115] the L_w + H + V[126] and L_w + H + L_{CO2}[127] hydrate equilibrium curves of the (CO_2 + H_2O) binary system, and the L_w + H + V hydrate curve for the (CH_4 + H_2O) binary system.[128]

The compositions of the three coexisting fluid phases have been obtained along eight isotherms at temperatures of (285.15, 287.65, 290.15, 292.65, 295.15, 297.65, 300.15, and 303.15) K and at pressures up to either the UCEP or the quadruple curve. Additionally, compositions of coexisting vapor and liquid phases have been measured along three isotherms at temperatures of (323.15, 373.15, and 423.15) K, pressures up to 20 MPa, and with the molar ratio between CO_2 and CH_4 kept roughly constant at about 0.5. The three- and four-phase states investigated are shown in Figure 3, and the experimental VLLE and VLE data are given in Tables 5 and 6 together with their estimated standard uncertainties. The quadruple curve along which hydrate coexists with the three fluid phases was also measured, and the results are presented in Table 7, while the UCEP data are given in Table 8.

4. MODELING

In this work, we used the SAFT-VR model to predict the VLLE using the parameters adopted by Míguez and co-workers,[44] which are based on those obtained by Clark et al.[129] for H_2O, Patel et al. for CH_4, [130] and Galindo and Blas for CO_2[131,132] from fits to vapor pressure and saturated liquid density data. Since, like any analytical equation of state, the SAFT approach does not reproduce the experimentally observed behavior close to the critical point, such fits are typically restricted to temperature below approximately $0.9T_c$, where T_c is the critical temperature. In order to obtain a good representation of the global phase diagram of the (CH_4 + CO_2 + H_2O) system, Míguez et al.[44] rescaled the parameters so as to reproduce the experimental critical temperature and pressure of each component. The resulting pure-component parameters are detailed in Table 9.

For the unlike (dispersion) energies, only the binary interaction parameter for the system CO_2−H_2O was considered; the value k_{ij} = 0.0258 was obtained by fitting to the experimental temperature minimum of the high-temperature branch of the fluid−fluid critical line.[44] All other cross-interaction parameters were obtained in the usual manner (using the Berthelot combining rule with k_{ij} = 0). This set of parameters was shown to provide an excellent description of the global phase diagram of this system over a wide range of temperatures. However, the model was not optimized for a quantitative description of the low-temperature mutual solubility data of the constituent binary subsystems, and low accuracy in the high-density region is also expected as a direct consequence of the rescaling of the parameters. The aim here was to compare the general experimental trends with a rigorous molecular-based equation of state such as SAFT-VR, focusing on the agreement in the high-temperature region and critical locus of the mixture.

For the calculation of hydrate-fluid equilibria, the SAFT-VR-based approach of Dufal et al.[45] was considered, along with the CSMHYD[48] model developed by the Colorado School of Mines. It should be noted that the SAFT-VR parameters used in the hydrate calculations are different from those given in Table 9 and their values may be found in ref 45. The reason for retaining the SAFT-VR parameters from ref 45 is that these values are consistent with the other parameters present in the model of Dufal et al.

5. DISCUSSION AND COMPARISON WITH EXPERIMENT

In Figure 4, we compare the two-phase VLE data with literature data and models.[32,112,114] In this figure, we plot the py_i/x_i for either CO_2 or CH_4 against the mole fraction of the other component, where x_i is the mole fraction of component i in the liquid phase and y_i is the mole fraction of the same component in the gas phase. This quantity is the apparent Henry's constant which we use as an inverse measure of solubility and a means of exploring the influence of adding a second nonaqueous component on the solubility of the first. Comparing our data at $y_1 \approx y_2 \approx 0.5$ with values calculated from the models of Duan et al.[112] at $y_1 = 0$ and Duan and Mao[114] at $y_2 = 0$, we see that in both cases the addition of the second nonaqueous component reduces the apparent Henry's constant and thus enhances the solubility of the first nonaqueous component, although this effect is quite small. In all cases, the apparent Henry's constant increases with pressure as expected from the finite partial molar volumes of CO_2 and CH_4 in the aqueous phase; the effect is more pronounced in the case of the CO_2. The only experimental data with which we can compare the present results are those of Qin et al.[32] at temperatures of (324.7 and 375.4) K and pressures between (20 and 50) MPa. Since the pressures considered in that work are higher than in the present

dx.doi.org/10.1021/jp509678g | J. Phys. Chem. B XXXX, XXX, XXX−XXX

Table 5. Experimental VLLE Data for [CH_4 (1) + CO_2 (2) + H_2O (3)] at Temperatures T and Pressures p, Where x_i Denotes the Mole Fraction of Component i and $u(x_i)$ Denotes Standard Uncertainty of x_i[a]

phase	p/MPa	x_1	$u(x_1)$	x_2	$u(x_2)$	x_3	$u(x_3)$
				T = 285.15 K			
I	4.963	0.0187	0.0013	0.9809	0.0014	0.000373	0.000009
II	4.961	0.00612	0.00039	0.98990	0.00039	0.003976	0.000089
III	4.957	0.000051	0.000004	0.02830	0.00062	0.97166	0.00062
I	5.538	0.0917	0.0017	0.9080	0.0017	0.000288	0.000007
II	5.529	0.02748	0.00057	0.9699	0.0058	0.002646	0.000059
III	5.525	0.000216	0.000006	0.02797	0.00061	0.97181	0.00061
I	6.381	0.1692	0.0022	0.8306	0.0022	0.000198	0.000005
II	6.384	0.06313	0.00098	0.93469	0.00099	0.002177	0.000049
III	6.379	0.000527	0.000012	0.02743	0.00060	0.97204	0.00061
I	7.077	0.2122	0.0025	0.7877	0.0025	0.000153	0.000005
II	7.075	0.0964	0.0014	0.9018	0.0014	0.001837	0.000040
III	7.070	0.000628	0.000014	0.02685	0.00059	0.97252	0.00060
				T = 287.65 K			
I	5.289	0.0243	0.0029	0.9754	0.0024	0.000366	0.000009
II	5.287	0.00736	0.00043	0.98949	0.00043	0.003148	0.000070
III	5.283	0.000051	0.000004	0.02770	0.00060	0.97225	0.00060
I	5.557	0.0495	0.0014	0.9502	0.0014	0.000296	0.000007
II	5.555	0.01766	0.00050	0.97970	0.00050	0.002644	0.000059
III	5.555	0.000127	0.000005	0.02755	0.00060	0.97232	0.00060
I	6.405	0.1283	0.0019	0.8715	0.0019	0.000206	0.000005
II	6.397	0.05155	0.00086	0.94626	0.00087	0.002196	0.000050
III	6.393	0.000394	0.000009	0.02705	0.00059	0.97256	0.00060
I	7.092	0.1769	0.0022	0.8230	0.0022	0.000154	0.000005
II	7.085	0.0834	0.0012	0.9147	0.0012	0.001916	0.000043
III	7.083	0.000557	0.000013	0.02647	0.00058	0.97297	0.00059
I	7.924	0.2158	0.0025	0.7841	0.0025	0.000110	0.000003
II	7.917	0.1318	0.0018	0.8664	0.0018	0.001767	0.000041
III	7.914	0.000755	0.000017	0.02560	0.00056	0.97365	0.00057
				T = 290.15 K			
I	5.693	0.03276	0.0012	0.96687	0.0012	0.000369	0.000009
II	5.690	0.01080	0.00048	0.98563	0.00048	0.003562	0.000082
III	5.689	0.000076	0.000004	0.02724	0.00060	0.97269	0.00060
I	5.725	0.03454	0.0012	0.96511	0.0013	0.000355	0.000009
II	5.725	0.01161	0.00049	0.98510	0.00049	0.003299	0.000075
III	5.725	0.000085	0.000004	0.02724	0.00059	0.97267	0.00060
I	6.117	0.06994	0.0014	0.92977	0.0014	0.000300	0.000007
II	6.114	0.02749	0.00062	0.96961	0.00063	0.002901	0.000066
III	6.111	0.000194	0.000006	0.02693	0.00059	0.97288	0.00059
I	6.555	0.11458	0.0017	0.88516	0.0017	0.000262	0.000007
II	6.548	0.04552	0.00081	0.95201	0.00082	0.002468	0.000057
III	6.551	0.000293	0.000007	0.02661	0.00058	0.97310	0.00058
I	7.176	0.15567	0.0020	0.84414	0.0020	0.000193	0.000005
II	7.177	0.07453	0.0011	0.92327	0.0012	0.002205	0.000051
III	7.179	0.000431	0.000010	0.02616	0.00057	0.97341	0.00058
I	7.275	0.16277	0.0021	0.83705	0.0021	0.000180	0.000005
II	7.265	0.07839	0.0012	0.91948	0.0012	0.002125	0.000048
III	7.269	0.000475	0.000011	0.02607	0.00057	0.97346	0.00058
I	7.927	0.18401	0.0022	0.81587	0.0022	0.000121	0.000003
II	7.930	0.11863	0.0016	0.87930	0.0016	0.002073	0.000048
III	7.926	0.000598	0.000032	0.02545	0.0016	0.97395	0.00058
				T = 292.65 K			
I	5.954	0.0225	0.0011	0.9771	0.0011	0.000364	0.000009
II	5.952	0.00828	0.00050	0.98836	0.00050	0.003363	0.000078
III	5.954	0.000055	0.000004	0.02664	0.00058	0.97331	0.00058
I	6.151	0.0392	0.0012	0.9605	0.0012	0.00034	0.000007
II	6.143	0.01589	0.00055	0.98100	0.00055	0.003112	0.000072
III	6.141	0.000101	0.000004	0.02653	0.00058	0.97337	0.00058
I	6.561	0.0760	0.0014	0.9237	0.0014	0.000281	0.000007
II	6.554	0.03412	0.00071	0.96298	0.00072	0.002893	0.000067

dx.doi.org/10.1021/jp509678g | J. Phys. Chem. B XXXX, XXX, XXX−XXX

Table 5. continued

phase	p/MPa	x_1	$u(x_1)$	x_2	$u(x_2)$	x_3	$u(x_3)$
				T = 292.65 K			
III	6.551	0.000205	0.000006	0.02621	0.00057	0.97359	0.00057
I	7.143	0.1214	0.0017	0.8784	0.0017	0.000221	0.000005
II	7.136	0.05794	0.00098	0.93959	0.00098	0.002464	0.000058
III	7.136	0.000345	0.000008	0.02574	0.00056	0.97392	0.00057
I	7.803	0.1541	0.0020	0.8459	0.0020	0.000152	0.000005
II	7.787	0.1023	0.0015	0.8955	0.0015	0.002186	0.000052
III	7.787	0.000481	0.000011	0.02497	0.00055	0.97455	0.00055
				T = 295.15 K			
I	6.2782	0.0207	0.0011	0.9790	0.0011	0.000370	0.000009
II	6.272	0.00803	0.00053	0.98779	0.00053	0.004176	0.000096
III	6.268	0.000046	0.000003	0.02575	0.00056	0.97421	0.00056
I	6.787	0.0632	0.0012	0.9365	0.0012	0.000302	0.000007
II	6.77	0.02843	0.00069	0.96817	0.00069	0.003399	0.000079
III	6.778	0.000160	0.000005	0.02543	0.00055	0.97441	0.00056
I	7.162	0.0920	0.0015	0.9077	0.0015	0.000247	0.000005
II	7.161	0.04523	0.00086	0.95157	0.00087	0.003196	0.000074
III	7.1595	0.000239	0.000006	0.02509	0.00057	0.97467	0.00055
I	7.7265	0.1192	0.0017	0.8806	0.0017	0.000189	0.000005
II	7.72	0.0745	0.0012	0.9226	0.0012	0.002981	0.000070
III	7.717	0.000366	0.000009	0.02457	0.00054	0.97506	0.00054
				T = 297.65 K			
I	6.675	0.02201	0.00098	0.97764	0.00098	0.000356	0.000009
II	6.675	0.01001	0.00058	0.98541	0.00058	0.00460	0.00011
III	6.6632	0.000056	0.000003	0.02493	0.00054	0.97502	0.00054
I	7.1773	0.0584	0.0011	0.9413	0.0011	0.000287	0.000007
II	7.1773	0.03046	0.00074	0.96556	0.00074	0.003973	0.000093
III	7.1595	0.000168	0.000005	0.02457	0.00053	0.97526	0.00053
I	7.7097	0.0856	0.0013	0.9142	0.0013	0.000219	0.000005
II	7.7019	0.0576	0.0010	0.9387	0.0010	0.003629	0.000084
III	7.6978	0.000273	0.000007	0.02407	0.00052	0.97566	0.00052
				T = 300.15 K			
I	7.1605	0.02751	0.00092	0.97218	0.00092	0.000313	0.000007
II	7.1528	0.01509	0.00064	0.97969	0.00065	0.00522	0.00011
III	7.153	0.000073	0.000003	0.02392	0.00052	0.97600	0.00052
I	7.612	0.0533	0.0010	0.9465	0.0010	0.000247	0.000005
II	7.603	0.03652	0.00082	0.95872	0.00083	0.00476	0.00011
III	7.602	0.000163	0.000005	0.02346	0.00051	0.97638	0.00051
				T = 300.50 K			
I	7.524	0.01357	0.00079	0.98611	0.00080	0.000324	0.000007
II	7.517	0.00934	0.00066	0.98503	0.00066	0.00563	0.00013
III	7.514	0.000038	0.000003	0.02307	0.00050	0.97690	0.00050

[a]The phases are labeled as I, II, and III for the gas, CO_2-rich liquid, and water-rich phases, respectively.

study, it is difficult to make a direct comparison. Nevertheless, the results of Qin et al. show a continuation of the trend whereby the apparent Henry's constant increases with pressure at constant temperature and constant y_1/y_2. In agreement with the present study, the results of Qin et al. also show a decrease in the effective Henry's constant upon the addition of a second nonaqueous component. Turning now to the predictions of the SAFT-VR model, we observe large differences from the experimental data with the predicted solubilities being too small by a large margin. This undoubtedly reflects the fact that the model was not tuned to any solubility data. The SAFT-VR calculations do mostly reflect the trends observed experimentally and come into somewhat better agreement as the temperature increases.

The present VLLE data are compared with the predictions of the SAFT-VR model in Figure 5 where we present isothermal (p, x_i) diagrams illustrating the compositions of the three coexisting phases. Parts a and b of Figure 5 show the solubilities of CH_4 and CO_2, respectively, in the aqueous phase under VLLE conditions. In common with the behavior observed in the two-phase region, these solubilities are strongly underpredicted by SAFT-VR. One can also observe that the mole fraction of CO_2 in the aqueous phase varies relatively little, being between 0.02 and 0.03 at all VLLE states investigated. In contrast, the mole fraction of CH_4 varies strongly with pressure across the VLLE region; at constant temperature, x_{CH_4} tends to zero at the lowest pressure and approaches its greatest value at the UCEP; at constant pressure, x_{CH_4} declines monotonically with increasing temperature toward zero at the high-temperature limit of three-phase coexistence. On average, x_{CH_4} is approximately 2 orders of magnitude smaller than x_{CO_2} in the

dx.doi.org/10.1021/jp509678g | J. Phys. Chem. B XXXX, XXX, XXX−XXX

Table 6. Experimental VLE Data for [CH_4 (1) + CO_2 (2) + H_2O (3)] at Temperatures T and Pressures p, Where x_i Denotes the Mole Fraction of Component i and $u(x_i)$ Denotes the Standard Uncertainty of x_i[a]

	phase II						phase III					
p/MPa	x_1	$u(x_1)$	x_2	$u(x_2)$	x_3	$u(x_3)$	x_1	$u(x_1)$	x_2	$u(x_2)$	x_3	$u(x_3)$
					T = 323.15 K							
1.911	0.4971	0.0035	0.4902	0.0035	0.01267	0.00028	0.000320	0.000012	0.003121	0.000077	0.996562	0.000081
6.035	0.4868	0.0036	0.5094	0.0036	0.00378	0.00011	0.000707	0.000016	0.00851	0.00019	0.99078	0.00021
10.011	0.4913	0.0036	0.5046	0.0036	0.00411	0.00011	0.000989	0.000022	0.01159	0.00026	0.98742	0.00028
14.021	0.5018	0.0037	0.4933	0.0038	0.00487	0.00012	0.001303	0.000031	0.01310	0.00029	0.98560	0.00032
17.986	0.4961	0.0039	0.4983	0.0039	0.00556	0.00014	0.001512	0.000033	0.01420	0.00032	0.98429	0.00034
					T = 373.15 K							
2.009	0.4727	0.0034	0.4615	0.0034	0.0658	0.0013	0.000235	0.000007	0.001831	0.000072	0.997942	0.000056
6.059	0.4864	0.0036	0.5033	0.0036	0.01028	0.00027	0.000681	0.000018	0.00529	0.00013	0.99403	0.00014
10.207	0.4915	0.0037	0.4978	0.0034	0.01068	0.00027	0.000941	0.000033	0.00840	0.00019	0.99066	0.00022
14.051	0.4814	0.0038	0.5073	0.0038	0.01125	0.00028	0.001107	0.000034	0.00981	0.00023	0.98908	0.00025
17.912	0.4835	0.0039	0.5044	0.0039	0.01207	0.00031	0.001315	0.000044	0.01181	0.00027	0.98688	0.00030
					T = 423.15 K							
2.102	0.3269	0.0034	0.3286	0.0034	0.3445	0.0048	0.000281	0.000008	0.001271	0.000089	0.998452	0.000064
4.201	0.3838	0.0034	0.3981	0.0034	0.2181	0.0036	0.000573	0.000014	0.002832	0.000099	0.996601	0.000084
5.956	0.4427	0.0034	0.4428	0.0034	0.1145	0.0021	0.001029	0.000023	0.00430	0.00013	0.99467	0.00013
9.982	0.4770	0.0036	0.4541	0.0035	0.0689	0.0014	0.001635	0.000035	0.00723	0.00018	0.99111	0.00019
14.061	0.4792	0.0037	0.4719	0.0037	0.0489	0.0010	0.001811	0.000033	0.00880	0.00021	0.98939	0.00023
18.001	0.4868	0.0039	0.4662	0.0039	0.04694	0.00099	0.001915	0.000042	0.01029	0.00025	0.98780	0.00027

[a]The phases are labeled as II and III for the CO_2-rich and water-rich phases respectively

Table 7. Experimental Quadruple Data for the Ternary System [CH_4 (1) + CO_2 (2) + H_2O (3)], Together with Predictions from Thermodynamic Models

	p/MPa		
T/K	expt	CSMHYD	SAFT-VR + vdWP
		This Work	
283.90	4.925	5.26	4.43
284.37	5.352	5.64	4.82
285.15	6.17	6.34	5.54
285.60	6.81	6.78	6.00
286.19	7.62	7.42	6.64
		Reference 43	
283.51	4.74	4.97	4.13
284.41	5.51	5.67	4.86
285.10	6.23	6.29	5.49
285.77	6.96	6.96	6.18
285.99	7.28	7.19	6.41
		References 38 and 42	
283.32	4.53	4.84	3.99
283.86	4.93	5.23	4.40
284.39	5.50	5.65	4.84
285.03	6.22	6.22	5.43
285.76	7.25	6.95	6.16

aqueous phase under VLLE conditions. Parts c and d of Figure 5 show the mole fractions of CH_4 and H_2O in the CO_2-rich liquid phase under VLLE conditions. Qualitatively, the mole fraction of CH_4 in the CO_2-rich liquid phase follows trends with temperature and pressure similar to those observed in the aqueous phase. On the other hand, the water content of the CO_2-rich liquid phase shows the reverse of these trends; for example, it decreases with increasing pressure along each isotherm under VLLE conditions. The mole fractions of both methane and water in the CO_2-rich liquid phase are slightly overestimated by SAFT-VR, but the agreement with experiment is much better than in the aqueous phase. In parts e and f of Figure 5, we plot the mole fractions of CO_2 and H_2O in the gas phase under VLLE conditions. The gas phase is also rich in CO_2, and the experimental CO_2 mole fractions are generally in good agreement with the SAFT-VR predictions. On the other hand, SAFT-VR strongly overestimates the mole fraction of H_2O in the gas phase. The amount of H_2O present in both the CO_2-rich liquid phase and the gas phase depends on the ratio of the mole fractions of CO_2 and CH_4 in that phase. We note that increasing the amount of CH_4 has the effect of decreasing the H_2O content of that phase. The same behavior was also observed by Song and Kobayashi[34] who concluded that the presence of the CH_4 lowered the H_2O content in the gas phase by 20% to 30% compared with the (CO_2 + H_2O) binary system at the same temperature and pressure.

5.1. Influence of H_2O on the Phase Behavior of (CH_4 + CO_2). The amount of H_2O present in the CO_2-rich liquid and gas phases is generally small and is observed to increase as temperature increases and to decrease as pressure increases, with more H_2O dissolved in the CO_2-rich liquid phase than in the gas phase. The presence of water in the nonaqueous phases has only a small effect on their equilibrium compositions. This is illustrated in Figure 6a,b, which are pressure−composition diagrams for the coexisting CO_2-rich liquid and gas phases. Here we compare the present experimental data in the VLLE region with the predictions of the SAFT-VR model and the available experimental data for the (CO_2 + CH_4) binary system.[55,133] Figure 6a shows the isotherms at temperatures of 287.65 and 295.15 K, while Figure 6b shows the isotherms at T = 292.65 K and T = 295.15 K. As the temperatures increases, the saturated region shifts toward higher CO_2 concentration and becomes smaller in size until it vanishes at the CO_2 critical temperature. Comparing the present data with the literature results for the binary system, it can be seen that the effect of the presence of H_2O is small in the low-pressure region. However, there is a noticeable difference at higher pressures, especially close to the critical point, despite the diminishing H_2O content in both CO_2-rich liquid phase and gas phase.

dx.doi.org/10.1021/jp509678g | J. Phys. Chem. B XXXX, XXX, XXX−XXX

Table 8. Experimental LLE Data for [CH_4 (1) + CO_2 (2) + H_2O (3)] at the Upper Critical End Point at Temperatures T and Pressures p, Where x_i Denotes the Mole Fraction of Component i and $u(x_i)$ Denotes Standard Uncertainty of x_i[a]

		phase II						phase III					
T/K	p/MPa	x_1	$u(x_1)$	x_2	$u(x_2)$	x_3	$u(x_3)$	x_1	$u(x_1)$	x_2	$u(x_2)$	x_3	$u(x_3)$
287.65	8.268	0.1979	0.0024	0.8021	0.0024	0.000069	0.000011	0.000852	0.000019	0.02559	0.00056	0.97356	0.00057
290.15	8.186	0.1716	0.0021	0.8283	0.0021	0.000090	0.000014	0.000704	0.000016	0.02493	0.00054	0.97437	0.00056
292.65	8.084	0.1403	0.0018	0.8596	0.0018	0.000116	0.000019	0.000569	0.000013	0.02470	0.00054	0.97473	0.00055
295.15	7.964	0.1109	0.0016	0.8889	0.0016	0.000148	0.000023	0.000428	0.000009	0.02448	0.00053	0.97509	0.00054
297.65	7.861	0.0826	0.0013	0.9173	0.0013	0.000183	0.000027	0.000314	0.000007	0.02433	0.00053	0.97536	0.00054
300.15	7.751	0.05421	0.00098	0.94558	0.00098	0.000215	0.000031	0.000193	0.000005	0.02417	0.00053	0.97564	0.00053
303.50	7.615	0.01621	0.00069	0.98354	0.00068	0.000256	0.000032	0.000056	0.000003	0.02410	0.00052	0.97585	0.00053

[a]The phases are labeled as II and III for the CO_2-rich liquid and water-rich phases, respectively.

It can be observed that the SAFT-VR predictions are excellent for the composition of the gas phase but somewhat less accurate for the coexisting liquid, especially at higher pressures and in the critical region. Deviations between theory and experiment in the composition at given conditions of temperature and pressure are of course expected at high-density conditions and in the critical region because of the limitations of the rescaling of parameters, which only ensures adjustment to the experimental critical temperature and pressure (but not density or, in the case of mixtures, composition).

The UCEP data are shown in Figure 7 in comparison with the predictions of the SAFT-VR model of Míguez and co-workers.[44] The agreement between theory and experiment is, in this case, excellent. Also plotted in Figure 7 are experimental VL critical points[133,134,138,139] for the (CO_2 + CH_4) binary system and the predicted critical curve of that binary mixture obtained from the GERG-2008 model of Kunz and Wagner.[135] It can be seen that the effect on the critical locus of water as a third component is very small indeed, again showing that small amounts of water have only a minor influence on the miscibility of CO_2 and CH_4.

In addition, comparing the influence of H_2O on the phase behavior of the present system with that on the phase behavior of the binaries (propane + CO_2),[28] (*n*-decane + CO_2), [27] and (*n*-heptane + CO_2)[29] leads to the conclusion that generally addition of H_2O has a small effect on the phase behavior of (*n*-alkane + CO_2) mixtures at temperatures well below the critical temperature of H_2O. In these systems, it can also be observed that the water content of the nonaqueous phases decreases as one moves toward lighter *n*-alkanes.

5.2. Influence of CH_4 on the Phase Behavior of (CO_2 + H_2O). The influence of CH_4 on the mutual solubility of (CO_2 + H_2O) is studied by comparison with the phase behavior of the (CO_2 + H_2O) binary system. For purposes of this comparison, we use the models developed by Duan et al.[112] and Spycher et al.[113] for the (CO_2 + H_2O) mixture. In Figure 8, we compare the K values of CO_2 and H_2O determined from the present VLLE data with those predicted by the models of Duan et al. and Spycher et al. at the same temperature and pressure. Under these conditions, the binary system is in the liquid−liquid region so the K values plotted are defined as $K_i = x_i^{II}/x_i^{III}$, where x_i^{II} denotes the mole fraction of component i in phase II (CO_2-rich liquid) and x_i^{III} denotes the mole fraction of component i in phase III (H_2O-rich liquid). Figure 8a shows K_{CO_2} as a function of pressure, and the agreement with both models is found to be good. Thus, by this comparison, the solubility of CO_2 in the aqueous phase appears to be slightly enhanced by the addition of methane.

Figure 8b shows K_{H_2O} as a function of pressure in comparison with the predictions of the models of Duan et al. and Spycher et al.[112,113,] However, Duan et al. adopted an approximate treatment for the composition of the CO_2-rich liquid phase, and they did not validate their model against experimental data in that regard. This perhaps explains the large differences observed in the calculated K values from the two models, and, for this reason, we prefer the model of Spycher et al. Thus, by comparison with the K_{H_2O} values predicted by the model of Spycher et al., the presence of H_2O in the CO_2-rich liquid phase appears to be —in general—slightly reduced by the addition of methane.

The CO_2 solubility in the H_2O-rich phase for (CH_4 + CO_2 + H_2O) is compared in Figure 9 with the measurements reported

dx.doi.org/10.1021/jp509678g | J. Phys. Chem. B XXXX, XXX, XXX−XXX

Table 9. SAFT-VR Parameters Used in This Work[a]

compound	ref	m	σ_{ii}/Å	(ε_{ii}/k_B)/K	λ_i	$(\varepsilon_{ii}^{HB}/k_B)$/K	K^{HB}/Å^3
CH_4	130	1.0	4.058	156.46	1.448		
CO_2	131,132	2.0	3.136	168.84	1.515		
H_2O	129	1.0	3.470	276.24	1.718	1229.27	1.3379

[a] m_i is the number of square-well segments in the molecule, σ_{ii} is the hard-core diameter, λ_{ii} and ε_{ii} are the range and the depth of the square-well potential, and ε_{ii}^{HB} and K^{HB} are the depth and the bonding volume of the four-site hydrogen-bonding interaction. Parameters have been rescaled to match the experimental critical temperature and pressure.

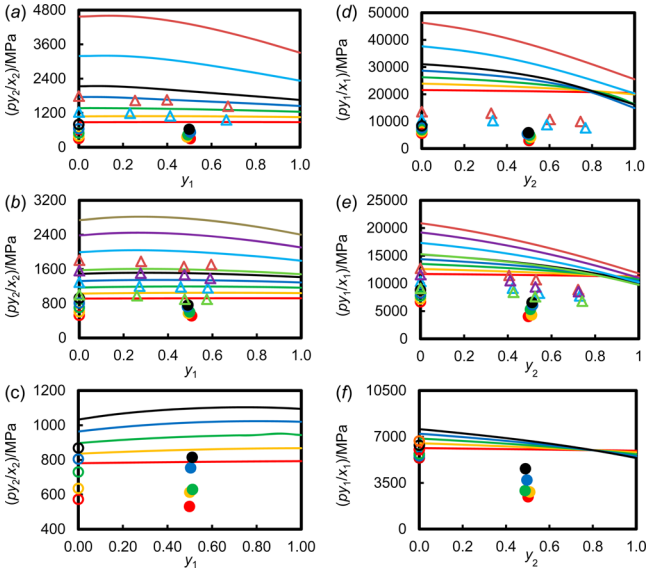

Figure 4. Apparent Henry's constant of CO_2 (a–c) and CH_4 (d–f) as a function of methane (y_1) or CO_2 (y_2) mole fraction in the gas phase under VLE conditions at T = 323.15 K (a and d), T = 373.15 K (b and e), and T = 423.15 K (c and f). Filled circles correspond to the data gathered in this work, open circles were obtained from the models of Duan et al.[112] and Duan and Mao,[114] open triangles are data from the literature,[32] and solid lines were calculated from the SAFT-VR model. Pressures are denoted by color as follows: 2 MPa (red); 6 MPa (orange); 10 MPa (green); 14 MPa (blue); 18 MPa (black); 20 MPa (light green); 30 MPa (light blue); 40 MPa (purple); 50 MPa (brown).

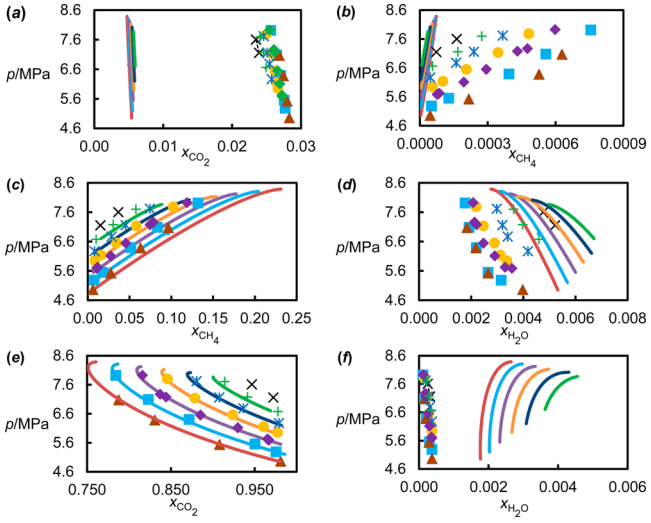

Figure 5. Isothermal pressure–composition (p, x) phase diagram for the (CH_4 + CO_2 + H_2O) system in the water-rich phase (a, b), CO_2-rich liquid phase (c, d), and gas phase (e, f) under VLLE conditions. Symbols correspond to the data gathered in this work at the following temperatures: ▲, T = 285.15 K; ■, T = 287.65 K; ♦, T = 290.15 K; ●, T = 292.65 K; *, T = 295.15 K; +, T = 297.65 K; ×, T = 300.15 K. The continuous curves are SAFT-VR predictions of the three-phase equilibrium region at T = 285.15 K (brown), T = 287.65 K (light blue), T = 290.15 K (purple), T = 292.65 K (orange), T = 295.15 K (dark blue), and T = 297.65 K (green).

by Forte et al.[27,28] for the (n-C_3H_8 + CO_2 + H_2O) and (n-$C_{10}H_{22}$ + CO_2 + H_2O) systems, by Brunner et al.[14] for (n-$C_{16}H_{34}$ + CO_2 + H_2O), and by Al Ghafri[29] for (n-C_7H_{16} + CO_2 + H_2O). In this figure, we plot the K value as $K_i = x_i^I/x_i^{III}$, where superscript I denotes the phase richest in alkane. It can be observed in Figure 9a that the K value of CO_2 decreases along an isotherm with increasing amount of alkane present in the alkane-rich phase. Thus, by this measure, the solubility of CO_2 in the aqueous phase appears to be enhanced by the addition of alkanes, and the latter can therefore be described as mild cosolvent for CO_2 in the aqueous phase. Figure 9b shows that the K value of CO_2 mostly increases with pressure along an isotherm. The present results are somewhat exceptional in this regard as they exhibit a slight decline with pressure along isotherms; however, the phase richest in alkane is in this case a gas phase whereas in the other systems is a liquid phase.

5.3. Influence of CO_2 on the Phase Behavior of (CH_4 + H_2O). The influence of CO_2 on the mutual solubility of (CH_4 + H_2O) is studied by comparison with the phase behavior of the (CH_4 + H_2O) binary system. For purposes of this comparison, we use the model developed by Duan and Mao[114] for the (CH_4 + H_2O) mixture. In Figure 10, we compare the K values of CH_4 and H_2O determined from the present VLLE data with those predicted by the model of Duan and Mao at the same temperature and pressure. Under these conditions, the binary system is in the vapor–liquid region so the K values plotted are defined as $K_i = x_i^I/x_i^{III}$. Figure 10a shows K_{CH_4} as a function of pressure, and we see that the experimental values in the ternary system under VLLE conditions are about half those of the corresponding binary mixture at the same temperature and pressure. This large difference partially reflects the very different chemical environment of the CH_4 molecule in the nonaqueous phase. In the case of the ternary mixture under VLLE conditions, we have a gas phase that is of the order of 90 mol % CO_2, whereas for the corresponding (CH_4 + H_2O) binary system the gas phase is more than 99 mol % CH_4. Calculations with the GERG-2008 model[135] show that the partial fugacity coefficient of CH_4 in the gas phase at the median VLLE conditions of the present study is about one-third larger than in the gas phase of the (CH_4 + H_2O) binary system at the same temperature and pressure. However, this factor alone does not explain the large differences illustrated in Figure 10a, so we can deduce that the presence of CO_2 in the aqueous phase acts as a significant cosolvent for methane dissolution in the aqueous phase. The same observation was made with the other ternary mixtures of the type (n-alkane +

dx.doi.org/10.1021/jp509678g | J. Phys. Chem. B XXXX, XXX, XXX–XXX

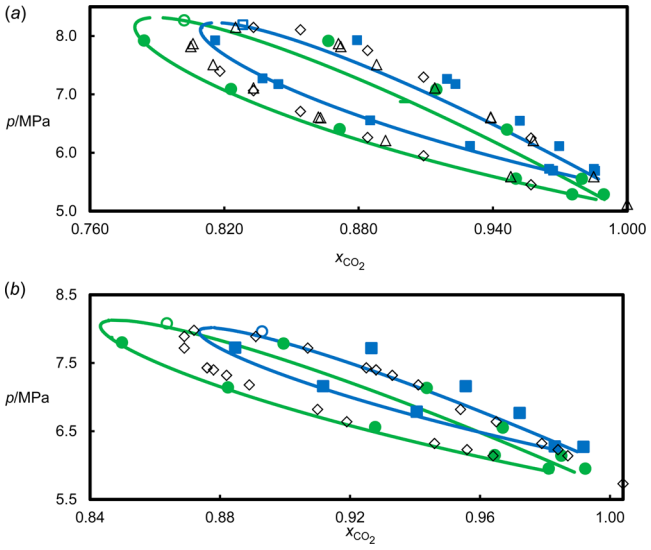

Figure 6. Isothermal pressure−composition phase diagram for the (CH_4 + CO_2 + H_2O) system at (a) T = 287.65 K (green) and T = 290.15 K (blue) and (b) T = 292.65 K (green) and T = 295.15 K (blue). Filled symbols correspond to the coexisting-phase data measured in this work, open colored symbols denote UCEP, and continuous curves correspond to SAFT-VR. Open black symbols correspond to published data for the binary system (CH_4 + CO_2): for a, (Δ) T = 288.55 K[55] and (◊) T = 288.15 K and for b, (◊) T = 293.4 K.[133]

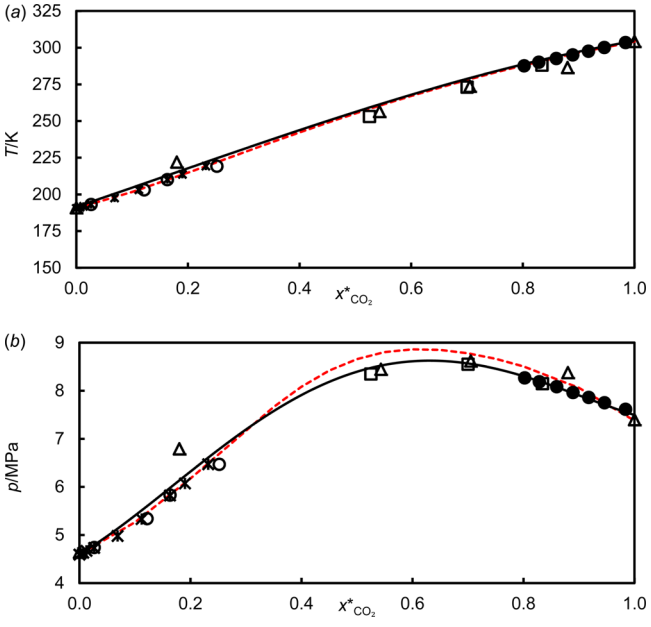

Figure 7. Plot showing the UCEP temperatures (a) and pressures (b) as a function of x^* = $x(CO_2)/[x(CH_4) + x(CO_2)]$: ●, this work for the ternary mixture (CH_4 + CO_2 + H_2O); □, ref 133; Δ, ref 137; *, ref 138; ○, ref 139. Critical data for the binary mixture (CH_4 + CO_2); solid and dotted lines represent the binary critical curve obtained from SAFT-VR[44] and GERG-2008, [135] respectively.

CO_2 + H_2O), and we conclude the presence of CO_2 generally increases the solubility of *n*-alkanes in water. In Figure 10b, K_{H_2O} is plotted against the pressure and compared with values calculated from the model of Duan and Mao[114] for the (CH_4 + H_2O) binary system. Since in both cases, the liquid phase contains more than 97 mol % water, it seems likely that the

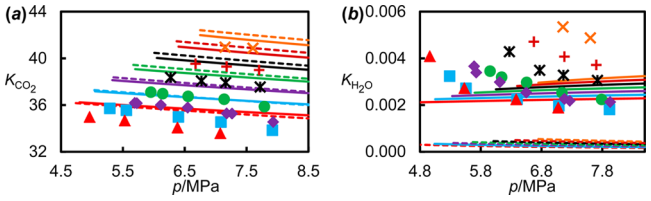

Figure 8. K factor of either CO_2 (a) or H_2O (b) as a function of pressure. Symbols correspond to the data of this work under VLLE conditions at the following temperatures: ▲, T = 285.15 K; ■, T = 287.65 K; ♦, T = 290.15 K; ●, T = 292.65 K; *, T = 295.15 K; +, T = 297.65 K; ×, T = 300.15 K. Dotted and continuous curves represent binary data for the system (CO_2 + H_2O) obtained from the models of Duan et al.[112] and Spycher et al.,[113] respectively, at the corresponding temperatures (indicated by color).

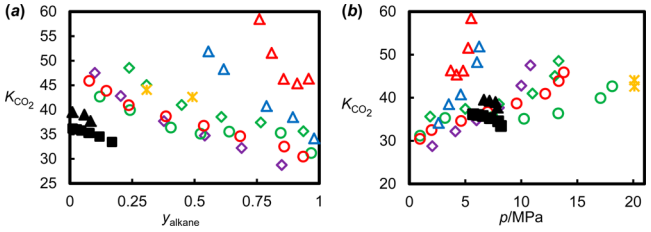

Figure 9. K factor of CO_2 in the hydrocarbon-rich phase under VLLE conditions as a function of (a) alkane mole fraction and (b) pressure. Filled symbols represent VLLE data gathered during this work at the following temperatures: ■, T = 290.15 K; ▲, T = 297.65 K. Open symbols represent literature data for other (*n*-alkane + CO_2 + H_2O) systems at temperatures of 338 K (blue), 343 K (purple), 353 K (red), 413 K (green), and 473 K (orange): Δ, propane;[28] ◊, heptane;[29] ○, decane;[27] *, hexadecane[14].

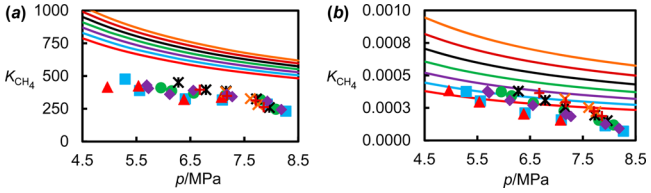

Figure 10. K factor of either CH_4 (a) or H_2O (b) as a function of pressure under VLLE conditions. Symbols correspond to the data of this work at the following temperatures: ▲, T = 285.15 K; ■, T = 287.65 K; ♦, T = 290.15 K; ●, T = 292.65 K; *, T = 295.15 K; +, T = 297.65 K; ×, T = 300.15 K. Continuous curves show the model of Duan and Mao[114] for the binary system (CH_4 + H_2O) at the corresponding temperatures (indicated by color).

differences observed in Figure 10b are associated mainly with molecular interactions in the gas phase where again we have very different chemical environments in the gas phases of the binary and ternary systems.

5.4. Four-Phase Line. The experimental data for the quadruple curve, including the vapor-phase composition, are given in Table 7, together with the experimental results obtained by Bi et al.[43] and Seo et al.[38,42] The quadruple curve data obtained in the present study agree well with the data of Bi et al.[43] and Seo et al.[38,42] At the lower end, this curve intersects the three-phase L_w + L_{CO_2} + V curve of the (CO_2 + H_2O) binary system at its quadruple point H + L_w + L_{CO_2} + V while, at its upper end, it meets the UCEP locus L_w + L_{CO_2} = V. The vapor compositions on the four-phase line were obtained by extrapolation of the experimental data measured in the three-

dx.doi.org/10.1021/jp509678g | J. Phys. Chem. B XXXX, XXX, XXX−XXX

phase region. These data were first interpolated on each isotherm to the experimental four-phase pressures and then extrapolated with respect to temperature by means of fitting quadratic polynomials for each isobar. It can be clearly seen that there is good agreement between our values and literature data both in terms of equilibrium conditions and vapor compositions.

Table 7 also shows the predictions of the CSMHYD[48] and SAFT-VR-vdWP[45] models. In both of these models, structure I hydrates are predicted with the larger cavities filled mainly with CO_2. The CSMHYD model actually predicts a range of pressures at given temperature over which four phases are predicted; the values given in Table 7 relate to the lowest predicted pressure. The agreement with experiment is then quite good. The SAFT-VR-vdWP predictions are (0.5 to 1.0) MPa lower than experiment.

6. CONCLUSION

In this work, we present the first comprehensive experimental investigation of phase equilibria of the (CH_4 + CO_2 + H_2O) system in the region where three fluid phases coexist. The three-phase VLLE data were gathered on eight isotherms at temperatures from (285.15 to 303.5) K and at pressures from roughly the vapor pressure of pure CO_2 up to either the upper critical end point (UCEP) or up to the hydrate formation locus. The quadruple curve along which hydrates coexist with the three fluid phases was also measured, and compositions of the coexisting vapor and liquid phases have been obtained along three isotherms at temperatures from (323.15 to 423.15) K and pressures up to 20 MPa.

The VLLE and VLE data have been compared with the predictions of the SAFT-VR making use of the model parameters reported previously by Míguez and co-workers.[44] Although this model does not provide a very accurate quantitative description of the phase behavior in either the VLE or the VLLE regions, it does predict the global phase diagram rather well and it must be recognized that the model was not tuned to any mixture data other than the VL critical curve of the (CO_2 + H_2O) binary subsystem. No doubt, much better quantitative agreement could be obtained by means of optimizing the binary parameters. The present experimental data should provide a strong basis for tuning and validating SAFT models in the future.

A detailed analysis of the ternary mixtures was carried out based on comparison with available data and models for the constituent binary subsystems and other ternary mixtures of the type (alkane + CO_2 + H_2O). It was concluded that the presence of CO_2 significantly increases the *n*-alkane solubility in the H_2O-rich phase under both VLE and VLLE conditions as compared to the corresponding (*n*-alkane + H_2O) binary system. In addition, the presence of *n*-alkane increases the CO_2 solubility in the H_2O-rich phase compared to the binary mixture of (CO_2 + H_2O) for both VLE and VLLE measurements. It was also concluded that the H_2O content in the CO_2-rich phase decreases in the presence of *n*-alkane as compared to the binary system of (CO_2 + H_2O). It was found that the effect of H_2O on the phase behavior (*n*-alkane + CO_2) was quite small, reflecting the low mole fraction of water in the nonaqueous phases. Finally, it was observed that predictions of the CSMHYD and SAFT-VR-vdWP hydrate models agree reasonably well with the experimental hydrate locus data. However, these models predict only three phases in equilibrium which does not agree with the experimental observations. Clearly the models require further refinement to be able to describe the full range of phase behavior observed for the (CH_4 + CO_2 + H_2O) system.

AUTHOR INFORMATION

Corresponding Author

*E-mail: m.trusler@imperial.ac.uk.

Notes

The authors declare no competing financial interest.

ACKNOWLEDGMENTS

This work was carried out as part of the activities of the Qatar Carbonates & Carbon Storage Research Centre (QCCSRC). We gratefully acknowledge the funding of QCCSRC provided jointly by Qatar Petroleum, Shell, and the Qatar Science and Technology Park, and their permission to publish this research. We also acknowledge the help of M.Sc. student Hak Lui in performing some of the VLLE measurements. In addition, we are pleased to acknowledge Dr. Andrew Haslam and Dr. Simon Dufal for running the SAFT-VR-vdWP hydrate model calculations.

REFERENCES

(1) Nagarajan, N. R.; Honarpour, M. M.; Sampath, K. Reservoir-fluid sampling and characterization-key to efficient reservoir management. *J. Pet. Technol.* **2007**, *59*, 80−91.

(2) Jaubert, J.-N.; Avaullee, L.; Souvay, J.-F. A crude oil data bank containing more than 5000 PVT and gas injection data. *J. Pet. Sci. Technol.* **2002**, *34*, 65−107.

(3) Jaubert, J.-N.; Avaullee, L.; Pierre, C. Is it still necessary to measure the minimum miscibility pressure? *Ind. Eng. Chem. Res.* **2001**, *41*, 303−310.

(4) Jaubert, J.-N.; Arras, L.; Neau, E.; Avaullee, L. Properly defining the classical vaporizing and condensing mechanisms when a gas is injected into a crude oil. *Ind. Eng. Chem. Res.* **1998**, *37*, 4860−4869.

(5) Neau, E.; Avaullée, L.; Jaubert, J. N. A new algorithm for enhanced oil recovery calculations. *Fluid Phase Equilib.* **1996**, *117*, 265−272.

(6) Jaubert, J.-N.; Neau, E.; Avaullee, L.; Zaborowski, G. Characterization of heavy oils. 3. Prediction of gas injection behavior: swelling test, multicontact test, multiple-contact minimum miscibility pressure, and multiple-contact minimum miscibility enrichment. *Ind. Eng. Chem. Res.* **1995**, *34*, 4016−4032.

(7) Manrique, E. J.; Thomas, C. P.; Ravikiran, R.; Kamouei, M. I.; Lantz, M.; Romero, J. L.; Alvarado, V., EOR: Current status and opportunities. *SPE improved oil recovery symposium*; SPE: Tulsa, OK, USA, 2010.

(8) Surguchev, D. L.; Manrique, D. E.; Alvarado, P. V. *Improved oil recovery: status and opportunities*, 18th World Petroleum Congress; World Petroleum Council: London, 2005.

(9) Holstein, E. D. *Status and outlook for enhanced oil recovery by chemical injection*; American Petroleum Institute: Washington, DC, USA, 1982.

(10) Henry, J. D. *Status and outlook for oil recovery using carbon dioxide injection operations*; American Petroleum Institute: Washington, DC, USA, 1981.

(11) Brashear, J. P.; Kuuskraa, V. A. The potential and economics of enhanced oil recovery. *J. Pet. Technol.* **1978**, *30*, 1231−1239.

(12) Ghedan, S. G. Global laboratory experience of CO_2-EOR flooding. *SPE/EAGE reservoir characterization and simulation conference*; SPE: Abu Dhabi, UAE, 2009.

(13) Aarnes, J.; Carpenter, M.; Flach, T.; Solomon, S.; Sollie, O. K.; Johnsen, K.; Rsnes, O. *CO2QUALSTORE: Guideline for selection and qualification of sites and projects for geological storage of CO_2*; DNV Technical Report 2009-1425; Det Norske Veritas: Bærum, Norway, 2009

(14) Brunner, G.; Teich, J.; Dohrn, R. Phase equilibria in systems containing hydrogen, carbon dioxide, water and hydrocarbons. *Fluid Phase Equilib.* **1994**, *100*, 253−268.
(15) Neau, E.; Jaubert, J. N.; Rogalski, M. Characterization of heavy oils. *Ind. Eng. Chem. Res.* **1993**, *32*, 1196−1203.
(16) Jaubert, J.-N.; Borg, P.; Coniglio, L.; Barth, D. Phase equilibria measurements and modeling of EPA and DHA ethyl esters in supercritical carbon dioxide. *J. Supercrit. Fluids* **2001**, *20*, 145−155.
(17) Chiu, H.-Y.; Jung, R.-F.; Lee, M.-J.; Lin, H.-M. Vapor−liquid phase equilibrium behavior of mixtures containing supercritical carbon dioxide near critical region. *J. Supercrit. Fluids* **2008**, *44*, 273−278.
(18) Eustaquio-Rincón, R.; Trejo, A. Solubility of n-octadecane in supercritical carbon dioxide at 310, 313, 333, and 353 K, in the range 10−20 MPa. *Fluid Phase Equilib.* **2001**, *185*, 231−239.
(19) Golombok, M.; Ineke, E.; Luzardo, J.-C.; He, Y.; Zitha, P. Resolving CO_2 and methane hydrate formation kinetics. *Environ. Chem. Lett.* **2009**, *7*, 325−330.
(20) Bruusgaard, H.; Beltrán, J. G.; Servio, P. Solubility measurements for the $CH_4 + CO_2 + H_2O$ system under hydrate−liquid−vapor equilibrium. *Fluid Phase Equilib.* **2010**, *296*, 106−109.
(21) Demirbas, A. Methane hydrates as potential energy resource: Part 2—Methane production processes from gas hydrates. *Energy Convers. Manage.* **2010**, *51*, 1562−1571.
(22) Demirbas, A. Methane hydrates as potential energy resource: Part 1—Importance, resource and recovery facilities. *Energy Convers. Manage.* **2010**, *51*, 1547−1561.
(23) W Taylor, F. The greenhouse effect and climate change. *Rep. Prog. Phys.* **1991**, *54*, No. 881.
(24) Thomas, S.; Dawe, R. A. Review of ways to transport natural gas energy from countries which do not need the gas for domestic use. *Energy* **2003**, *28*, 1461−1477.
(25) Linga, P.; Kumar, R.; Englezos, P. Gas hydrate formation from hydrogen/carbon dioxide and nitrogen/carbon dioxide gas mixtures. *Chem. Eng. Sci.* **2007**, *62*, 4268−4276.
(26) Sloan, E. D., Jr.; Koh, C. A. *Clathrate Hydrates of Natural Gases*; Taylor & Francis: Boca Raton, FL, USA, 2008.
(27) Forte, E.; Galindo, A.; Trusler, J. P. M. Experimental and molecular modeling study of the three-phase behavior of (*n*-decane + carbon dioxide + water) at reservoir conditions. *J. Phys. Chem. B* **2011**, *115*, 14591−14609.
(28) Forte, E.; Galindo, A.; Trusler, J. P. M. Experimental and molecular modelling study of the three-phase behaviour of (propane + carbon dioxide + water) at reservoir conditions. *J. Supercrit. Fluids* **2013**, *75*, 30−42.
(29) Al Ghafri, S. Z. S. Phase behaviour and physical properties of reservoir fluids under addition of carbon dioxide. Ph.D. Thesis, Imperial College London, London, 2013.
(30) Galindo, A.; Davies, L. A.; Gil-Villegas, A.; Jackson, G. The thermodynamics of mixtures and the corresponding mixing rules in the SAFT-VR approach for potentials of variable range. *Mol. Phys.* **1998**, *93*, 241−252.
(31) Gil-Villegas, A.; Galindo, A.; Whitehead, P. J.; Mills, S. J.; Jackson, G.; Burgess, A. N. Statistical associating fluid theory for chain molecules with attractive potentials of variable range. *J. Chem. Phys.* **1997**, *106*, 4168−4186.
(32) Qin, J. F.; Rosenbauer, R. J.; Duan, Z. Experimental measurements of vapor-liquid equilibria of the $H_2O + CO_2 + CH_4$ ternary system. *J. Chem. Eng. Data* **2008**, *53*, 1246−1249.
(33) Dhima, A.; de Hemptinne, J.-C.; Jose, J. Solubility of hydrocarbons and CO_2 mixtures in water under highpressure. *Ind. Eng. Chem. Res.* **1999**, *38*, 3144−3161.
(34) Song, K. Y.; Kobayashi, R. The water content of a carbon dioxide-rich gas mixture containing 5.31 Mol % methane along the three-phase and supercritical conditions. *J. Chem. Eng. Data* **1990**, *35*, 320−322.
(35) Jarne, C.; Blanco, S. T.; Gallardo, M. A.; Rauzy, E.; Otín, S.; Velasco, I. Dew points of ternary methane (or ethane) + carbon dioxide + water mixtures: Measurement and correlation. *Energy Fuels* **2004**, *18*, 396−404.
(36) Belandria, V.; Eslamimanesh, A.; Mohammadi, A. H.; Théveneau, P.; Legendre, H.; Richon, D. Compositional analysis and hydrate dissociation conditions measurements for carbon dioxide + methane + water system. *Ind. Eng. Chem. Res.* **2011**, *50*, 5783−5794.
(37) Beltrán, J. G.; Servio, P. Equilibrium studies for the system methane + carbon dioxide + neohexane + water. *J. Chem. Eng. Data* **2008**, *53*, 1745−1749.
(38) Seo, Y.-T.; Lee, H.; Yoon, J.-H. Hydrate phase equilibria of the carbon dioxide, methane, and water system. *J. Chem. Eng. Data* **2001**, *46*, 381−384.
(39) Ohgaki, K. T.; Sangawa, K.; Matsubara, H.; Nakano, T. S. Methane exploitation by carbon dioxide from gas hydrates-phase equilibria for CO_2−CH_4 mixed hydrate system. *J. Chem. Eng. Jpn.* **1996**, *29*, 478−483.
(40) Uchida, T.; Ikeda, I. Y.; Takeya, S.; Kamata, Y.; Ohmura, R.; Nagao, J.; Zatsepina, O. Y.; Buffett, B. A. Kinetics and stability of CH_4−CO_2 mixed gas hydrates during formation and long-term storage. *ChemPhysChem.* **2005**, *6*, 646−654.
(41) Mohammadi, A. H.; Anderson, R.; Tohidi, B. Carbon monoxide clathrate hydrates: Equilibrium data and thermodynamic modeling. *AlChE J.* **2005**, *51*, 2825−2833.
(42) Seo, Y.-T.; Lee, H. Multiple-phase hydrate equilibria of the ternary carbon dioxide, methane, and water mixtures. *J. Phys. Chem. B* **2001**, *105*, 10084−10090.
(43) Bi, Y.; Yang, T.; Guo, K. Determination of the upper-quadruple-phase equilibrium region for carbon dioxide and methane mixed gas hydrates. *J. Pet. Sci. Eng.* **2013**, *101*, 62−67.
(44) Míguez, J. M.; dos Ramos, M. C.; Piñeiro, M. M.; Blas, F. J. An examination of the ternary methane + carbon dioxide + water phase diagram using the SAFT-VR approach. *J. Phys. Chem. B* **2011**, *115*, 9604−9617.
(45) Dufal, S.; Galindo, A.; Jackson, G.; Haslam, A. J. Modelling the effect of methanol, glycol inhibitors and electrolytes on the equilibrium stability of hydrates with the SAFT-VR approach. *Mol. Phys.* **2012**, *110*, 1223−1240.
(46) van der Waals, J. H.; Platteeuw, J. C. Clathrate solutions. *Adv. Chem. Phys.* **1959**, 1−57.
(47) Platteeuw, J. C.; van der Waals, J. H. Thermodynamic properties of gas hydrates. *Mol. Phys.* **1958**, *1*, 91−96.
(48) Colorado School of Mine. CSMHYD, Available online: http://hydrates.mines.edu/CHR/Software.html; 1998.
(49) Mraw, S. C.; Hwang, S.-C.; Kobayashi, R. Vapor-liquid equilibrium of the methane-carbon dioxide system at low temperatures. *J. Chem. Eng. Data* **1978**, *23*, 135−139.
(50) Al Sahhaf, T. Liquid vapor equilibriums in the nitrogen carbon dioxide methane system. *Ind. Eng. Chem. Fundam.* **1983**, *22*, 372−380.
(51) Knapp, H.; Yang, X.; Zhang, Z. Vapor—liquid equilibria in ternary mixtures containing nitrogen, methane, ethane and carbon-dioxide at low temperatures and high pressures. *Fluid Phase Equilib.* **1990**, *54*, 1−18.
(52) Davalos, J. Liquid−vapor equilibria at 250.00.deg.K for systems containing methane, ethane, and carbon dioxide. *J. Chem. Eng. Data* **1976**, *21*, 81−84.
(53) Webster, L. A.; Kidnay, A. J. Vapor−Liquid Equilibria for the Methane−Propane−Carbon Dioxide Systems at 230 and 270 K. *J. Chem. Eng. Data* **2001**, *46*, 759−764.
(54) Somait. Liquid-vapor equilibriums at 270.00 K for systems containing nitrogen, methane, and carbon dioxide. *J. Chem. Eng. Data* **1978**, *23*, 301−305.
(55) Xu, N.; Dong, J.; Wang, Y.; Shi, J. High pressure vapor liquid equilibria at 293 K for systems containing nitrogen, methane and carbon dioxide. *Fluid Phase Equilib.* **1992**, *81*, 175−186.
(56) Bian, B.; Wang, Y.; Shi, J.; Zhao, E.; Lu, B. C. Y. Simultaneous determination of vapor-liquid equilibrium and molar volumes for coexisting phases up to the critical temperature with a static method. *Fluid Phase Equilib.* **1993**, *90*, 177−187.
(57) Addicks, J.; Owren, G. A.; Fredheim, A. O.; Tangvik, K. Solubility of carbon dioxide and methane in aqueous methyldiethanol-amine solutions. *J. Chem. Eng. Data* **2002**, *47*, 855−860.

(58) Awan, J. A.; Thomsen, K.; Coquelet, C.; Fosbøl, P. L.; Richon, D. Vapor−liquid equilibrium measurements and modeling of the propyl mercaptan + methane + water system. *J. Chem. Eng. Data* **2009**, *55*, 842−846.
(59) Chapoy, A.; Coquelet, C.; Richon, D. Solubility measurement and modeling of water in the gas phase of the methane/water binary system at temperatures from 283.08 to 318.12 K and pressures up to 34.5 MPa. *Fluid Phase Equilib.* **2003**, *214*, 101−117.
(60) Chapoy, A.; Mohammadi, A. H.; Richon, D.; Tohidi, B. Gas solubility measurement and modeling for methane−water and methane−ethane−n-butane−water systems at low temperature conditions. *Fluid Phase Equilib.* **2004**, *220*, 111−119.
(61) Chapoy, A.; Mohammadi, A. H.; Tohidi, B.; Richon, D. Estimation of water content for methane + water and methane + ethane + *n*-butane + water systems using a new sampling device. *J. Chem. Eng. Data* **2005**, *50*, 1157−1161.
(62) Crovetto, R. Solubilities of inert gases and methane in H_2O and in D_2O in the temperature range of 300 to 600 K. *J. Chem. Phys.* **1982**, *76*, 1077.
(63) Duffy, J. R.; Smith, N. O.; Nagy, B. Solubility of natural gases in aqueous salt solutions—I: Liquidus surfaces in the system CH_4-H_2O-$NaCl_2$-$CaCl_2$ at room temperatures and at pressures below 1000 psia. *Geochim. Cosmochim. Acta* **1961**, *24*, 23−31.
(64) Fenghour, A.; Wakeham, W. A.; Watson, J. T. R. Densities of (water + methane) in the temperature range 430 to 699 K and at pressures up to 30 MPa. *J. Chem. Thermodyn.* **1996**, *28*, 447−458.
(65) Folas, G. K.; Froyna, E. W.; Lovland, J.; Kontogeorgis, G. M.; Solbraa, E. Data and prediction of water content of high pressure nitrogen, methane and natural gas. *Fluid Phase Equilib.* **2007**, *252*, 162−174.
(66) Kiepe, J.; Horstmann, S.; Fischer, K.; Gmehling, J. Experimental determination and prediction of gas solubility data for CO_2 + H_2O mixtures containing NaCl or KCl at temperatures between 313 and 393 K and pressures up to 10 MPa. *Ind. Eng. Chem. Res.* **2002**, *41*, 4393−4398.
(67) Kim, Y. S.; Ryu, S. K.; Yang, S. O.; Lee, C. S. Liquid water−hydrate equilibrium measurements and unified predictions of hydrate-containing phase equilibria for methane, ethane, propane, and their mixtures. *Ind. Eng. Chem. Res.* **2003**, *42*, 2409−2414.
(68) Lekvam, K.; Bishnoi, P. R. Dissolution of methane in water at low temperatures and intermediate pressures. *Fluid Phase Equilib.* **1997**, *131*, 297−309.
(69) Yilin, W.; Buxing, H.; Haike, Y.; Ruilin, L. Solubility of CH_4 in the mixed solvent t-butyl alcohol and water. *Thermochim. Acta* **1995**, *253*, 327−334.
(70) Mohammadi, A. H.; Chapoy, A.; Richon, D.; Tohidi, B. Experimental measurement and thermodynamic modeling of water content in methane and ethane systems. *Ind. Eng. Chem. Res.* **2004**, *43*, 7148−7162.
(71) Sage, B. H.; Lacey, W. N. Phase equilibria in hydrocarbon systems I methods and apparatus. *Ind. Eng. Chem.* **1934**, *26*, 103−106.
(72) Siqueira Campos, C. E. P.; Penello, J. R.; Pellegrini Pessoa, F. L.; Cohen Uller, A. M. Experimental measurement and thermodynamic modeling for the solubility of methane in water and hexadecane. *J. Chem. Eng. Data* **2010**, *55*, 2576−2580.
(73) Rigby, M.; Prausnitz, J. M. Solubility of water in compressed nitrogen, argon, and methane. *J. Phys. Chem.* **1968**, *72*, 330−334.
(74) Servio, P.; Englezos, P. Measurement of dissolved methane in water in equilibrium with its hydrate. *J. Chem. Eng. Data* **2001**, *47*, 87−90.
(75) Shmonov, V. M.; Sadus, R. J.; Franck, E. U. High-pressure phase equilibria and supercritical pVT data of the binary water + methane mixture to 723 K and 200 MPa. *J. Phys. Chem. A* **1993**, *97*, 9054−9059.
(76) Yang, S. O.; Cho, S. H.; Lee, H.; Lee, C. S. Measurement and prediction of phase equilibria for water + methane in hydrate forming conditions. *Fluid Phase Equilib.* **2001**, *185*, 53−63.
(77) Yarrison, M.; Cox, K. R.; Chapman, W. G. Measurement and modeling of the solubility of water in supercritical methane and ethane from 310 to 477 K and pressures from 3.4 to 110 MPa. *Ind. Eng. Chem. Res.* **2006**, *45*, 6770−6777.
(78) Anderson, G. K. Solubility of carbon dioxide in water under incipient clathrate formation conditions. *J. Chem. Eng. Data* **2002**, *47*, 219−222.
(79) Bamberger, A.; Sieder, G.; Maurer, G. High-pressure (vapor +liquid) equilibrium in binary mixtures of (carbon dioxide+water or acetic acid) at temperatures from 313 to 353 K. *J. Supercrit. Fluids* **2000**, *17*, 97−110.
(80) Bando, S.; Takemura, F.; Nishio, M.; Hihara, E.; Akai, M. Solubility of CO_2 in aqueous solutions of NaCl at (30 to 60) °C and (10 to 20) MPa. *J. Chem. Eng. Data* **2003**, *48*, 576−579.
(81) Bermejo, M. D.; Martín, A.; Florusse, L. J.; Peters, C. J.; Cocero, M. J. The influence of Na_2SO_4 on the CO_2 solubility in water at high pressure. *Fluid Phase Equilib.* **2005**, *238*, 220−228.
(82) Briones, J. A.; Mullins, J. C.; Thies, M. C.; Kim, B. U. Ternary phase equilibria for acetic acid-water mixtures with supercritical carbon dioxide. *Fluid Phase Equilib.* **1987**, *36*, 235−246.
(83) Coan, C. R.; King, A. D. Solubility of water in compressed carbon dioxide, nitrous oxide, and ethane—Evidence for hydration of carbon dioxide and nitous oxide in gas phase. *J. Am. Chem. Soc.* **1971**, *93*, 1857−1862.
(84) Crovetto, R.; Wood, R. H. Solubility of CO_2 in water and density of aqueous CO_2 near the solvent critical temperature. *Fluid Phase Equilib.* **1992**, *74*, 271−288.
(85) Dalmolin, I.; Skovroinski, E.; Biasi, A.; Corazza, M. L.; Dariva, C.; Oliveira, J. V. Solubility of carbon dioxide in binary and ternary mixtures with ethanol and water. *Fluid Phase Equilib.* **2006**, *245*, 193−200.
(86) Dell'Era, C.; Uusi-Kyyny, P.; Pokki, J. P.; Pakkanen, M.; Alopaeus, V. Solubility of carbon dioxide in aqueous solutions of diisopropanolamine and methyldiethanolamine. *Fluid Phase Equilib.* **2010**, *293*, 101−109.
(87) Dohrn, R.; Bünz, A. P.; Devlieghere, F.; Thelen, D. Experimental measurements of phase equilibria for ternary and quaternary systems of glucose, water, CO_2 and ethanol with a novel apparatus. *Fluid Phase Equilib.* **1993**, *83*, 149−158.
(88) Ferrentino, G.; Barletta, D.; Donsí, F.; Ferrari, G.; Poletto, M. Experimental measurements and thermodynamic modeling of CO_2 solubility at high pressure in model apple juices. *Ind. Eng. Chem. Res.* **2010**, *49*, 2992−3000.
(89) Iwai, Y.; Uno, M.; Nagano, H.; Arai, Y. Measurement of solubilities of palmitic acid in supercritical carbon dioxide and entrainer effect of water by FTIR spectroscopy. *J. Supercrit. Fluids* **2004**, *28*, 193−200.
(90) Jackson, K.; Bowman, L. E.; Fulton, J. L. Water solubility measurements in supercritical fluids and high-pressure liquids using near-infrared spectroscopy. *Anal. Chem.* **1995**, *67*, 2368−2372.
(91) Jarne, C.; Blanco, S. T.; Artal, M.; Rauzy, E.; Otín, S.; Velasco, I. Dew points of binary carbon dioxide + water and ternary carbon dioxide + water + methanol mixtures: Measurement and modelling. *Fluid Phase Equilib.* **2004**, *216*, 85−93.
(92) King, M. B.; Mubarak, A.; Kim, J. D.; Bott, T. R. The mutual solubilities of water with supercritical and liquid carbon dioxide. *J. Supercrit. Fluids* **1992**, *5*, 296−302.
(93) Zawisza, A.; Malesinska, B. Solubility of carbon dioxide in liquid water and of water in gaseous carbon dioxide in the range 0.2−5 MPa and at temperatures up to 473 K. *J. Chem. Eng. Data* **1981**, *26*, 388−391.
(94) Martín, Á.; Pham, H. M.; Kilzer, A.; Kareth, S.; Weidner, E. Phase equilibria of carbon dioxide, poly ethylene glycol and water mixtures at high pressure: Measurements and modelling. *Fluid Phase Equilib.* **2009**, *286*, 162−169.
(95) Mather, A. E.; Franck, E. U. Phase equilibria in the system carbon dioxide-water at elevated pressures. *J. Phys. Chem.* **1992**, *96*, 6−8.
(96) Nakayama, T.; Sagara, H.; Arai, K.; Saito, S. High-pressure liquid-liquid equilibria for the system of water, ethanol and 1,1-difluroethane at *T* 323.2 K. *Fluid Phase Equilib.* **1987**, *38*, 109−127.

(97) Nighswander, J. A.; Kalogerakis, N.; Mehrotra, A. K. Solubilities of carbon dioxide in water and 1 wt. % sodium chloride solution at pressures up to 10 MPa and temperatures from 80 to 200.degree.C. *J. Chem. Eng. Data* **1989**, *34*, 355−360.
(98) Patel, M. R.; Holste, J. C.; Hall, K. R.; Eubank, P. T. Thermophysical properties of gaseous carbon dioxide and water mixtures. *Fluid Phase Equilib.* **1987**, *36*, 279−299.
(99) Campos, C.; Villardi, H. G. D.; Pessoa, F. L. P.; Uller, A. M. C. Solubility of carbon dioxide in water and hexadecane: Experimental measurement and thermodynamic modeling. *J. Chem. Eng. Data* **2009**, *54*, 2881−2886.
(100) Prutton, C. F.; Savage, R. L. The solubility of carbon dioxide in calcium chloride-water solutions at 75, 100, 120° and high pressures. *J. Am. Chem. Soc.* **1945**, *67*, 1550−1554.
(101) Qin, J.; Rosenbauer, R. J.; Duan, Z. Experimental measurements of vapor−liquid equilibria of the H_2O + CO_2 + CH_4 ternary system. *J. Chem. Eng. Data* **2008**, *53*, 1246−1249.
(102) Ruffine, L.; Trusler, J. P. M. Phase behaviour of mixed-gas hydrate systems containing carbon dioxide. *J. Chem. Thermodyn.* **2010**, *42*, 605−611.
(103) Servio, P.; Englezos, P. Effect of temperature and pressure on the solubility of carbon dioxide in water in the presence of gas hydrate. *Fluid Phase Equilib.* **2001**, *190*, 127−134.
(104) Silkenbäumer, D.; Rumpf, B.; Lichtenthaler, R. N. Solubility of carbon dioxide in aqueous solutions of 2-amino-2-methyl-1-propanol and *n*-methyldiethanolamine and their mixtures in the temperature range from 313 to 353 K and pressures up to 2.7 MPa. *Ind. Eng. Chem. Res.* **1998**, *37*, 3133−3141.
(105) Stewart, P. B.; Munjal, P. Solubility of carbon dioxide in pure water, synthetic sea water, and synthetic sea water concentrates at 5.deg. to 2.deg. and 10- to 45-atm. pressure. *J. Chem. Eng. Data* **1970**, *15*, 67−71.
(106) Takahashi, S.; Song, K. Y.; Kobayashi, R. Experimental vapor-liquid equilibriums in the carbon dioxide-diethylene glycol-water and carbon dioxide-triethylene glycol-water systems at feasible absorption temperatures and pressures. *J. Chem. Eng. Data* **1984**, *29*, 23−28.
(107) Teng, H.; Yamasaki, A.; Chun, M. K.; Lee, H. Solubility of liquid CO_2 in water at temperatures from 278 to 293 K and pressures from 6.44 to 29.49 MPa and densities of the corresponding aqueous solutions. *J. Chem. Thermodyn.* **1997**, *29*, 1301−1310.
(108) Valtz, A.; Chapoy, A.; Coquelet, C.; Paricaud, P.; Richon, D. Vapour-liquid equilibria in the carbon dioxide-water system, measurement and modelling from 278.2 to 318.2K. *Fluid Phase Equilib.* **2004**, *226*, 333−344.
(109) Zheng, D.-Q.; Guo, T.-M.; Knapp, H. Experimental and modeling studies on the solubility of CO_2, CHC_1F_2, CHF_3, $C_2H_2F_4$ and $C_2H_4F_2$ in water and aqueous NaCl solutions under low pressures. *Fluid Phase Equilib.* **1997**, *129*, 197−209.
(110) Hou, S.-X.; Maitland, G. C.; Trusler, J. P. M. Measurement and modeling of the phase behavior of the (carbon dioxide + water) mixture at temperatures from 298.15 to 448.15 K. *J. Supercrit. Fluids* **2013**, *73*, 87−96.
(111) Duan, Z.; Sun, R. An improved model calculating CO_2 solubility in pure water and aqueous NaCl solutions from 273 to 533 K and from 0 to 2000 bar. *Chem. Geol.* **2003**, *193*, 257−271.
(112) Duan, Z.; Sun, R.; Zhu, C.; Chou, I. M. An improved model for the calculation of CO_2 solubility in aqueous solutions containing Na^+, K^+, Ca^{2+}, Mg^{2+}, Cl^-, and SO_4^{2-}. *Mar. Chem.* **2006**, *98*, 131−139.
(113) Spycher, N.; Pruess, K.; Ennis-King, J. CO_2-H_2O mixtures in the geological sequestration of CO_2. I. Assessment and calculation of mutual solubilities from 12 to 100°C and up to 600 bar. *Geochim. Cosmochim. Acta* **2003**, *67*, 3015−3031.
(114) Duan, Z.; Mao, S. A thermodynamic model for calculating methane solubility, density and gas phase composition of methane-bearing aqueous fluids from 273 to 523 K and from 1 to 2000 bar. *Geochim. Cosmochim. Acta* **2006**, *70*, 3369−3386.
(115) Span, R.; Wagner, W. A new equation of state for carbon dioxide covering the fluid region from the triple-point temperature to 1100 K at pressures up to 800 MPa. *J. Phys. Chem. Ref. Data* **1996**, *25*, 1509−1596.
(116) Setzmann, U.; Wagner, W. A new equation of state and tables of thermodynamic properties for methane covering the range from the melting line to 625 K at pressures up to 100 MPa. *J. Phys. Chem. Ref. Data* **1991**, *20*, 1061−1155.
(117) Schedemann, A.; Ihmels, E. C.; Gmehling, J. Liquid densities of THF and excess volumes for the mixture with water in a wide temperature and pressure range. *Fluid Phase Equilib.* **2010**, *295*, 201−207.
(118) Ohmura, R.; Takeya, S.; Uchida, T.; Ebinuma, T. Clathrate hydrate formed with methane and 2-propanol: Confirmation of structure II hydrate formation. *Ind. Eng. Chem. Res.* **2004**, *43*, 4964−4966.
(119) *Evaluation of measurement data—Guide to the expression of uncertainty in measurement*, JCGM 100:2008; Joint Committee for Guides in Metrology, BIPM: Sèvres, France, 2008.
(120) D'Souza, R.; Patrick, J. R.; Teja, A. S. High pressure phase equilibria in the carbon dioxide-n-Hexadecane and carbon dioxide-water systems. *Can. J. Chem. Eng.* **1988**, *66*, 319−323.
(121) Webster, L. A. Vapor−liquid equilibria for the methane−propane−carbon dioxide systems at 230 and 270 K. *J. Chem. Eng. Data* **2001**, *46*, 759.
(122) Brunner, E. Fluid mixtures at high pressures IX. Phase separation and critical phenomena in 23 (n-alkane + water) mixtures. *J. Chem. Thermodyn.* **1990**, *22*, 335−353.
(123) Scott, R. L.; van Konynenburg, P. H. Critical lines and phase equilibria in binary Van der Waals mixtures. *Philos. Trans. R. Soc., A* **1980**, *298*, 495−540.
(124) Scott, R. L.; van Konynenburg, P. H. Static properties of solutions. Van der Waals and related models for hydrocarbon mixtures. *Discuss. Faraday Soc.* **1970**, *49*, 87−97.
(125) Bluma, M.; Deiters, U. K. A classification of phase diagrams of ternary fluid systems. *Phys. Chem. Chem. Phys.* **1999**, *1*, 4307−4313.
(126) Robinson, D. B.; Metha, B. R. Hydrates In the propane-carbon dioxide-water system. *J. Can. Pet. Technol.* **1971**, *10*, 33−35.
(127) Takenouchi, S.; Kennedy, G. C. The binary system H_2O-CO_2 at high temperatures and pressures. *Am. J. Sci.* **1964**, *262*, 1055−1074.
(128) Nakamura, T.; Makino, T.; Sugahara, T.; Ohgaki, K. Stability boundaries of gas hydrates helped by methane—Structure-H hydrates of methylcyclohexane and cis-1,2-dimethylcyclohexane. *Chem. Eng. Sci.* **2003**, *58*, 269−273.
(129) Clark, G. N. I.; Haslam, A. J.; Galindo, A.; Jackson, G. Developing optimal wertheim-like models of water for use in statistical associating fluid theory (SAFT) and related approaches. *Mol. Phys.* **2006**, *104*, 3561−3581.
(130) Patel, B. H.; Paricaud, P.; Galindo, A.; Maitland, G. C. Prediction of the salting-out effect of strong electrolytes on water + alkane solutions. *Ind. Eng. Chem. Res.* **2003**, *42*, 3809−3823.
(131) Galindo, A.; Blas, F. J. Theoretical examination of the global fluid phase behavior and critical phenomena in carbon dioxide + *n*-alkane binary mixtures. *J. Phys. Chem. B* **2002**, *106*, 4503−4515.
(132) Blas, F. J.; Galindo, A. Study of the high pressure phase behaviour of CO_2+n-alkane mixtures using the SAFT-VR approach with transferable parameters. *Fluid Phase Equilib.* **2002**, *194−197*, 501−509.
(133) Arai, Y.; Kaminishi, G.; Saito, S. The experimental determination of the P-V-T-x relations for the carbon dioxide-nitrogen and the carbon dioxide-methane systems. *J. Chem. Eng. Jpn.* **1971**, *4*, 113−122.
(134) Donnelly, H. G.; Katz, D. L. Phase equilibria in the carbon dioxide−methane system. *Ind. Eng. Chem.* **1954**, *46*, 511−517.
(135) Kunz, O.; Wagner, W. The GERG-2008 wide-range equation of state for natural gases and other mixtures: An expansion of GERG-2004. *J. Chem. Eng. Data* **2012**, *57*, 3032−3091.
(136) Gil, L.; Avila, S.; García-Giménez, P.; Blanco, S. T.; Berro, C.; Otin, S.; Velasco, I. Dew points of binary propane or *n*-butane + carbon dioxide, ternary propane or *n*-butane + carbon dioxide + water, and quaternary propane or *n*-butane + carbon dioxide + water +

methanol mixtures: Measurement and modeling. *Ind. Eng. Chem. Res.* **2006**, *45*, 3974−3980.
(137) Donnelly, H. G.; Katz, D. L. Phase equilibria in the carbon dioxide−methane system. *Ind. Eng. Chem.* **1954**, *46*, 511−517.
(138) Hwang, S. C.; Lin, H.-O.; Chappelear, P.; Kobayashi, R. *Dew-point values for the methane-carbon dioxide system*, RR-21; Gas Processors Association: Tulsa, OK, USA, 1976
(139) Mraw, S. C.; Hwang, S. C. *The vapor-liquid equilibrium of the CH4-CO2 system at low temperatures*, RR-25; Gas Processors Association: Tulsa, OK, USA, 1977; 118